BBA - Biomembranes 1863 (2021) 183715

Contents lists available at ScienceDirect

BBA - Biomembranes

journal homepage: www.elsevier.com/locate/bbamem

Anthrax toxin channel: What we know based on over 30 years of research

Wenxing Liu, Ekaterina M. Nestorovich *

Department of Biology, The Catholic University of America, 620 Michigan Ave, Washington, DC 20064, USA

ARTICLE INFO

Keywords:
Tripartite anthrax toxin
Protein translocation
Channel-mediated transport
Protein fluctuation dynamics
Ion channel conductance
Targeted toxin

ABSTRACT

Protective antigen channel is the central component of the deadly anthrax exotoxin responsible for binding and delivery of the toxin's enzymatic lethal and edema factor components into the cytosol. The channel, which is more than three times longer than the lipid bilayer membrane thickness and has a 6-Å limiting diameter, is believed to provide a sophisticated unfoldase and translocase machinery for the foreign protein transport into the host cell cytosol. The tripartite toxin can be reengineered, one component at a time or collectively, to adapt it for the targeted cancer therapeutic treatments. In this review, we focus on the biophysical studies of the protective antigen channel-forming activity, small ion transport properties, enzymatic factor translocation, and blockage comparing it with the related clostridial binary toxin channels. We address issues linked to the anthrax toxin channel structural dynamics and lipid dependence, which are yet to become generally recognized as parts of the toxin translocation machinery.

1. Introduction

The focus of this review written for the thematic "*Mechanisms of function and regulation of large transport membrane channels*" issue of the Journal is on the protective antigen (PA) component of anthrax exotoxin, or rather on its 63-kDa fragment (PA_{63}), which oligomerizes to form a translocation channel (Fig. 1, *left*) to transport the two ~90-kDa enzymatic components of the toxin into the cytosol of target cells. Because mushroom-like shape and oligomeric structure of PA_{63} resembles those of the well-known α-hemolysin (αHL) of *Staphylococcus aureus* [1] (Fig. 1, *right*), in the past these two bacterial toxin channel-forming proteins were frequently compared. An immediate practical purpose of such a comparison was to suggest moving aside from investigating the PA_{63}'s role in the toxin uptake and exploring it as a potential model channel-forming protein in various biophysical applications focusing on its ion and macromolecule sensing and transport properties. Thus, at least within the community of ion channel researchers, αHL is recognized mainly not as an *S. aureus* virulent exotoxin but as a protein nanopore suitable for biosensing applications, with the nucleic acid sequencing studies being one of the most prominent examples [2–4]. Yet, despite some structural similarities, the molecular sensing properties of PA_{63} and αHL are very distinct. The purpose of this review is to summarize the existing research on the anthrax toxin channel properties performed in planar lipid bilayers (PLM), to discuss the accumulated data on its role in the enzymatic component transport, and to highlight those unique characteristics of the channel that can foreordain its greater use as a model system to investigate molecular mechanisms of channel-facilitated ion and macromolecular transport.

2. Anthrax toxin structure, assembly, and function

Anthrax toxin is an AB type tripartite exotoxin secreted by a large Gram-positive, rod-shaped, spore-forming aerobic bacterium, *Bacillus anthracis*. The toxin is composed of two enzymatic A components, Lethal Factor (LF) and Edema Factor (EF), and one binding and translocation B component, Protective Antigen, that self-assemble at the host cell surface forming two "classic" binary toxins, lethal toxin (LT = LF + PA) and edema toxin (ET = EF + PA) contributing to the anthrax symptoms. Lethal Factor is a Zn-metalloprotease, which disturbs host cell signal transduction by cleaving mitogen-activated protein kinase kinases (MAPKKs) and Nlrp1 [6–8]. Edema Factor is a Ca^{2+} and calmodulin-dependent adenylyl cyclase that elevates intracellular cAMP level, contributing to the dissemination of *B. anthracis* in the host [9,10]. Protective Antigen, named because of its long-lasting use as an active component of the vaccine against anthrax, is a host cell receptor binding and translocation component responsible for the LF and EF intracellular entry, which occurs in several stages (Fig. 2).

Host cell delivery of the anthrax toxin is achieved through clathrin [12] and receptor-mediated endocytosis [13]. First, an 83-kDa full-length PA (PA_{83}) binds to its specific cellular tumor endothelial

* Corresponding author.
E-mail address: Nestorovich@cua.edu (E.M. Nestorovich).

https://doi.org/10.1016/j.bbamem.2021.183715
Received 20 March 2021; Received in revised form 21 July 2021; Accepted 24 July 2021
Available online 30 July 2021

marker-8 (TEM8) (also known as ANTXR1) and capillary morphogenesis gene 2 (CMG2) (also known as ANTXR2) receptors [14–20]. The receptors discovered in the early 2000s (reviewed in refs. [21–23]), were recently shown to be linked to recessive autosomal diseases. CMG2 mutations resulted in hyaline fibromatosis syndrome [24,25] and TEM8 mutations in GAPO (growth retardation, alopecia, pseudo-anodontia, and optic atrophy) syndrome [26]. After cleavage to PA_{63} by the furin-like proteases and release of PA_{20} [27], receptor-bound PA_{63} self-assembles forming ring-shaped heptameric, $(PA_{63})_7$, [28] and/or octameric, $(PA_{63})_8$, prepores [29] on the host cell surface. The prepore formation generates three (in $(PA_{63})_7$) [30] and four (in $(PA_{63})_8$) [29] sites for the LF and/or EF binding. The anthrax toxin complexes are then endocytosed [31] and transited from the early to late endosomal multivesicular compartments under the lowering endosomal pH environment, first encountering the early endosome (EE) pH ~ 5.5–6.0 and then in the late endosome (LE) pH ~ 5.0–5.5. The acidic conditions trigger substantial conformational changes in the PA_{63} oligomeric prepores resulting in their insertion into endosomal membranes and formation of elongated transmembrane pores [5,28]. It was reported that the pH threshold required for the prepore – pore transition is different depending on the cellular receptor PA_{83} originally binds, with pH 6.3 being sufficient to weaken the PA_{63}/TEM8 contact but lower pH 5.2 needed to weaken the PA_{63}/CMG2 contact [16–18]. This finding may indicate a possibility for the TEM8-bound PA_{63} to form channels already at the early endosomal stages, whereas the lower late endosomal pH is probably required for the CMG2-bound PA_{63} transitioning to the channel [19,20]. The formed PA_{63} channel was described to work as an effective translocate, responsible for unfolding LF and EF and translocating them into the cytosol, where they catalyze the host cell disrupting reactions. The process is powered by the pH gradient across the endosomal limiting membranes [32,33].

Several alternative or complementary assembly and translocation mechanisms were suggested. Thus, PA_{63} was shown to oligomerize jointly with PA_{83} [34]. The authors detected the formation of $LF_1(PA_{83})_2(PA_{63})_5$ and $LF_1(PA_{83})_1(PA_{63})_6$ mixed complexes with retained cytotoxic effects. It was suggested that these functional complexes may form under the conditions of furin deficiency, *e.g.*, under terminal stages of anthrax when the PA_{83} levels exceed those of the proprotein convertase. In another study, PA_{63} monomers were shown to bind directly to the full-length LF or LF_N, although their binding affinity was lower compared to the oligomeric prepore interaction [35]. The authors also reported that it is possible that some PA_{20} fragments remain non-covalently bound to PA_{63}, suggesting that PA_{20} may act as a hook to bind LF molecules pulling them in from extracellular surroundings. Apart from translocating LF across the endosomal limiting membranes, anthrax toxin complexes were also suggested to insert preferentially into endosomal intraluminal vesicles delivering LF into their lumen (Fig. 2) [36,37]. If so, these vesicles can fully protect LF from proteolytic degradation, delivering it into the cytosol *via* fusion at a much later time. Moreover, an alternative anthrax toxin uptake model suggests that instead of the PA-mediated LF and EF translocation, the toxin delivers its enzymatic cargo by catalyzing the endosomal membranes rupture [38].

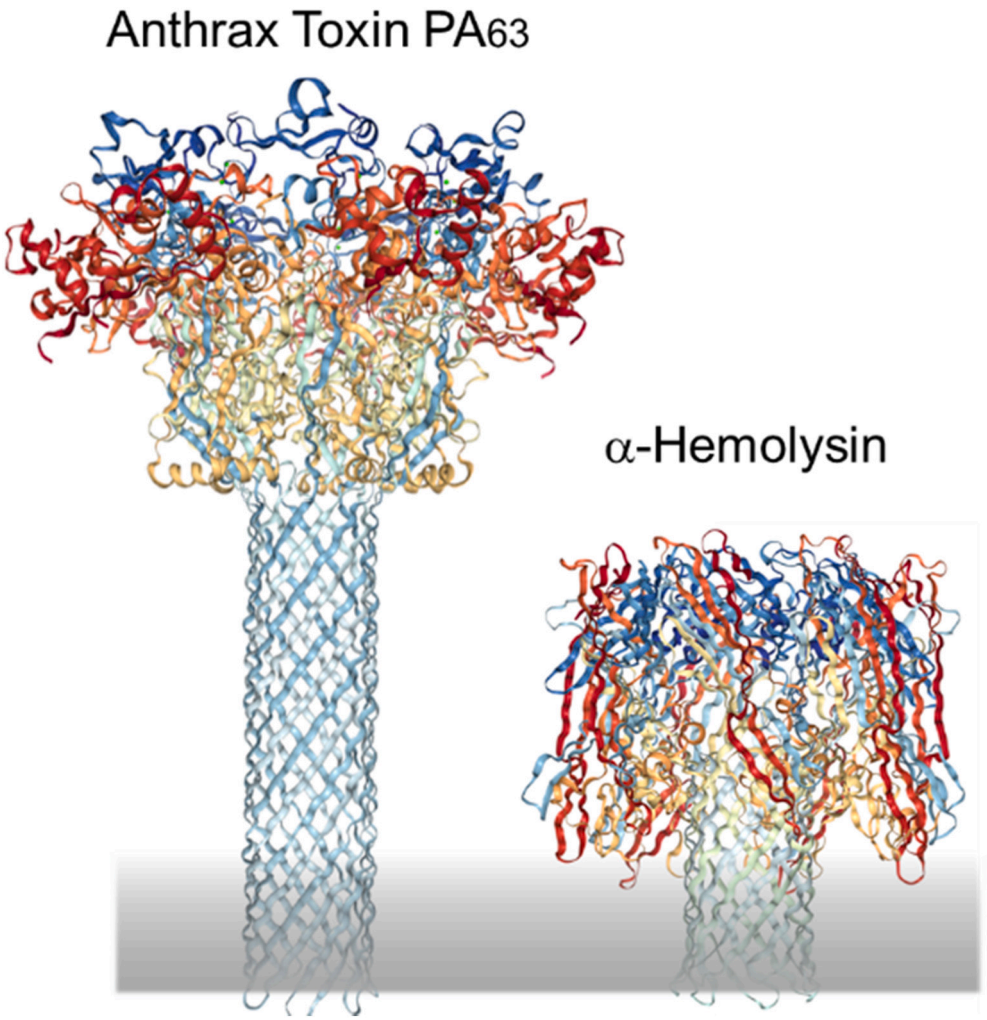

Fig. 1. *Bacillus anthracis* PA_{63}, 3J9C [5] (*left*), and *Staphylococcus aureus* αHL, 7AHL [1] (*right*) channel-forming exotoxin proteins plotted at the same scale.

3. PA_{63}, an elongated channel with unique properties

Protective antigen is the central component of the anthrax toxin, responsible for LF and EF translocation into the cytosol. A monomeric PA is a 735 amino acid (83 kDa) protein composed of four structural domains, D1-D4 [28]. An amino-terminal domain 1 (residues 1–249) contains two calcium ions and a furin protease cleavage site, which divides it into two sub-domains, a 20-kDa domain D1a, which diffuses away and an LF/EF binding domain D1b. A channel-forming domain D2 (residues 250–487) contains a flexible loop associated with membrane insertion. Domain D3 is the smallest domain (residues 488–594) associated with oligomerization. Finally, domain D4 (residues 595–735) is a receptor-binding domain, which has little contact with the remaining domains. While the full-length PA_{83} binds to its cellular receptors, it cannot oligomerize forming a water-soluble channel because of steric hindrance between the D1a subdomains. After proteolytic cleavage and D1a removal, PA oligomerizes and, following $(PA_{63})_7(LF/EF)_3$ and $(PA_{63})_8(LF/EF)_4$ complex formation, undergoes endocytosis (Fig. 2). The oligomeric PA_{63} forms a water-filled single-tunnel channel connecting aqueous solutions on both sides of the endosomal membrane. Interestingly, the channel is more than 3 times longer than the thickness of a lipid bilayer membrane; PA_{63} is an extended ~180-Å-long 14-strand β-barrel [28] channel, which was compared to a flower a stem, with a 75 Å-long bud and a 105 Å-long stem (Fig. 1, *left*) and internal radius varying from 3 Å to 16 Å [5]. Starting from 1989 [39], the PA_{63} channel properties have been studied extensively *in vitro* using the PLM technique where PA, cleaved to PA_{63}, was shown to spontaneously form stable highly cation-selective voltage-gated ion channels under the sub-acidic pH conditions [40–43]. In addition, recent technical advances in cryo-electron microscopy have allowed for determining high-resolution structures of $(PA_{63})_7$ channel [5], $(PA_{63})_7LF_3$ prepores [44], $(PA_{63})_8(LF/EF)_4$ prepores [45], and $(PA_{63})_7$ channels with partially unfolded LF and EF bound [46].

3.1. PA_{63} channel formation

The PA_{63} channel-forming activity was reported to be pH-dependent; generally, it required mildly acidic pH for the ion channels to form *in vitro*. Structural details of the prepore/pore conformational switch, together with numerous other aspects of the anthrax toxin formation and internalization, were reviewed recently by Liddington [47]. While the channel formation was detected between the pH range of 4 to 7.5 [11], the channel activity was considerably increased at the sub-acidic pH range of 5 to 6.5 (*cis* - *trans* symmetric) and substantially decreased in neutral (pH: 7–7.5) and acidic (pH $\leq$ 4.5) solutions [11,39]. This finding is in agreement with the endosomal pH acidification needed for the PA_{63} channels to form. Yet, the transmembrane pH gradient, existing between the endosomal membranes, did not seem to be important for the channel reconstitution in the *in vitro* studies. Moreover, neither the interaction with the host cell receptors nor the LF and EF component binding were required for the channel formation in PLMs [39].

3.2. PA_{63} channel oligomeric state

For a long time, the population of oligomeric PA_{63} channels was believed to be exclusively heptameric, as detected using the X-ray PA_{63} prepore [28] and cryo-EM PA_{63} channel [5] 7-fold symmetric atomic structures. Then, the formation of functional octameric, or 8-fold symmetric form, was discovered and investigated [29,48–50]. Comparison of the heptameric and octameric prepore crystal structures showed that in the octamers there are two types of PA monomer conformations

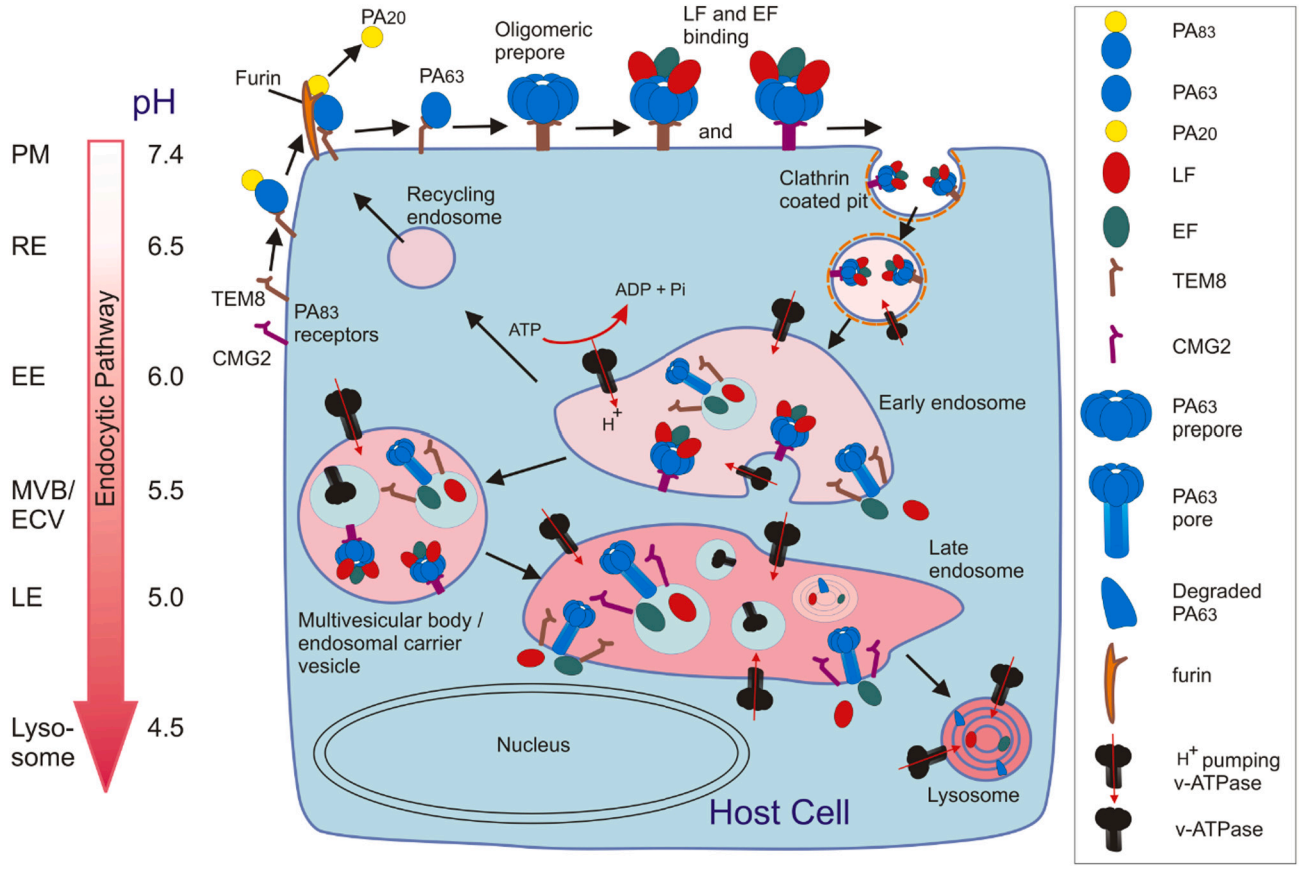

Fig. 2. Schematic representation of the anthrax toxin internalization process.
Modified with permission from ref. [11].Copyright (2017) John Wiley and Sons and Copyright Clearance Center.

occupying alternating positions in the ring [29]. It is unclear if the wild type $(PA_{63})_8$-WT channels were ever reconstituted and recorded in PLMs (see the related discussion in Section 3.3 below). However, Phillips et al. engineered anthrax toxin variants that complemented each other pairwise to selectively and exclusively form octamers (Fig. 3) [51]. These PA variants were individually unable to form channels but demonstrated the channel-forming activity when combined with their complementary partners. The authors selected an oligomerization-deficient PA-D512K mutant (Fig. 3, *top*) and then designed a library of individually inactive complementary mutants (Fig. 3, *middle*) choosing four positively charged residues on the opposite face of PA within 6 Å of the D512K mutation looking for the "gain of function" mutations (Fig. 3, *bottom*). The engineered individually non-toxic PA-K245G/R252N and PA-K245N/R252S variants, referred to as PA-GN and PA-NS, when combined with PA-D512K, generated high toxicity comparable to that of the PA-WT. Evidence of assembly of the octamers was obtained using electron microscopy and electrophysiological measurements; the latter showed single (PA-GN + PA-D512K) and (PA-NS + PA-D512K) 8-fold symmetric constructs having, respectively, ~8% and ~16% greater conductance compared to the 7-fold symmetric PA-WT. The octamer strategy was designed to create tumor-targeting anthrax toxin constructs with high specificity and efficacy (see Section 3.7 below for more details).

3.3. PA_{63} channel conductance

In PLMs, PA_{63} has been shown to form approximately ohmic channels with relatively small, compared to other β-barrel channels, conductance, ~180 pS in 1 M KCl at pH 6.6 [40]. Just to give a few examples, the single-channel conductances of the mitochondrial outer membrane VDAC, outer membrane trimeric OmpF of *E.coli*, and aforementioned α-HL of *S. aureus*, measured under similar conditions, are ~4.0 pS [52], 1.4 nS (given per monomer) [53], and 1.0 nS [54] correspondingly. The low conductivity of PA_{63} was linked to the presence of a steric bottleneck [55] formed by a narrow ring of hydrophobic phenylalanine 427 side chains (the so-called ϕ-clamp) [56] situated at the connection of the channel's bud and stem. Indeed, the PA_{63}-F427A mutant's conductance is about three times higher compared to PA_{63}-WT [56,57]. Moreover, the single PA_{63} current profile possesses several unique and very interesting features.

3.3.1. *The 'maximum' and 'main' conductance states and the two PA_{63} insertion types*

PA_{63} channels were reported to exhibit spontaneous reversible stepwise transitions to a higher conductance state [40,58] (labeled as states 'main' and 'max' in Fig. 4A). The inserting channels were frequently detected as being in the 'max' conductance state but then quickly (seconds or faster) changing to the 'main' conductance state [11]. The 'max' state could later reappear, as seen at the pH 6.5 single PA_{63} channel current recording (Fig. 4A, *top*). The relative probabilities of the two conductance states varied significantly from channel to channel, but the 'main' state was typically predominant. Das and Krantz hypothesized [59] that the alternate PA_{63} conductance states represent the so-called 'clamped empty' and 'unclamped empty dilated' states of the channel, with the dilation occurring at the ϕ-clamp (Fig. 4B) [56]. The idea originated with an attempt to provide support for the allosteric

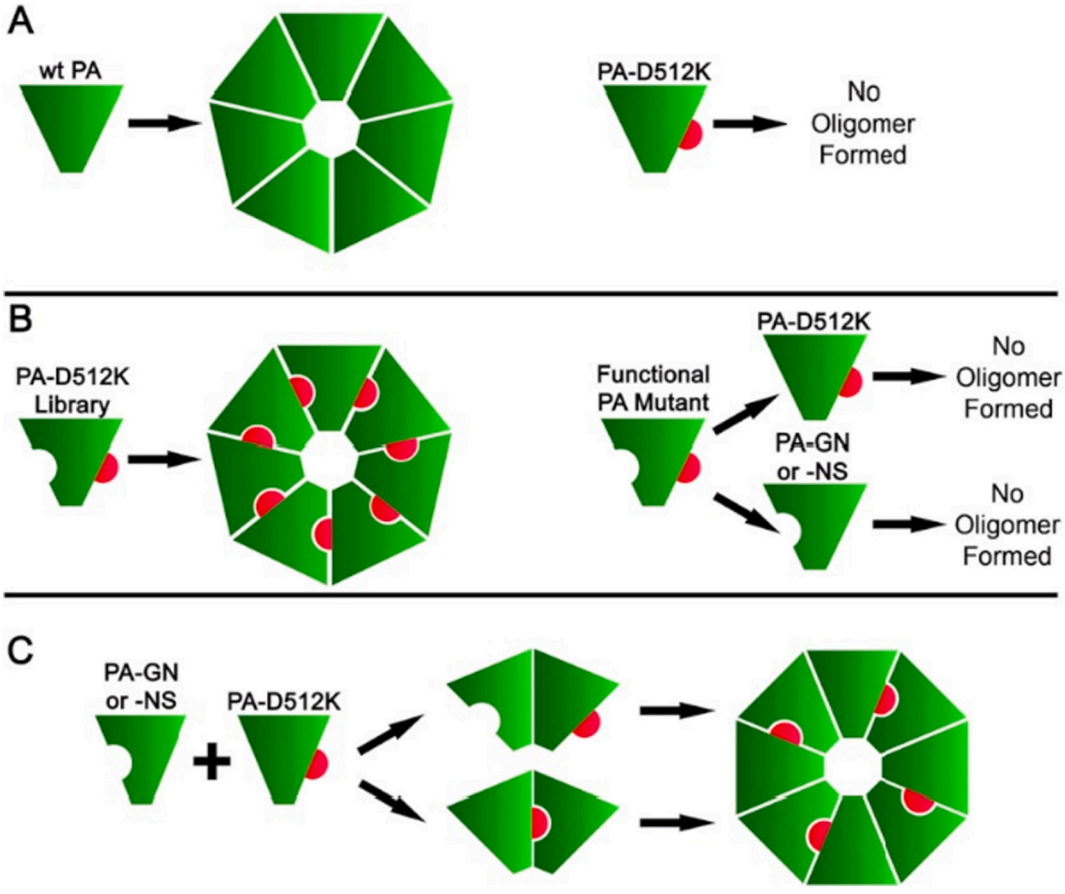

Fig. 3. Design of PA_{63} mutants, exclusively forming octamers. *Top*: PA_{63}-WT oligomerizes forming heptamers (*left*), however, PA_{63}-D512K is oligomerization-deficient (*right*). *Middle*: A library of PA-D512K mutants with an additional gain of function mutation (*left*); the mutations are then separated between different PA monomers (*right*). *Bottom*: Combining the complementary PA_{63} variants allows for the formation of heterogenous 4:4 octamers.
Reprinted with permission from ref. [51]. Copyright (2013) Elsevier.

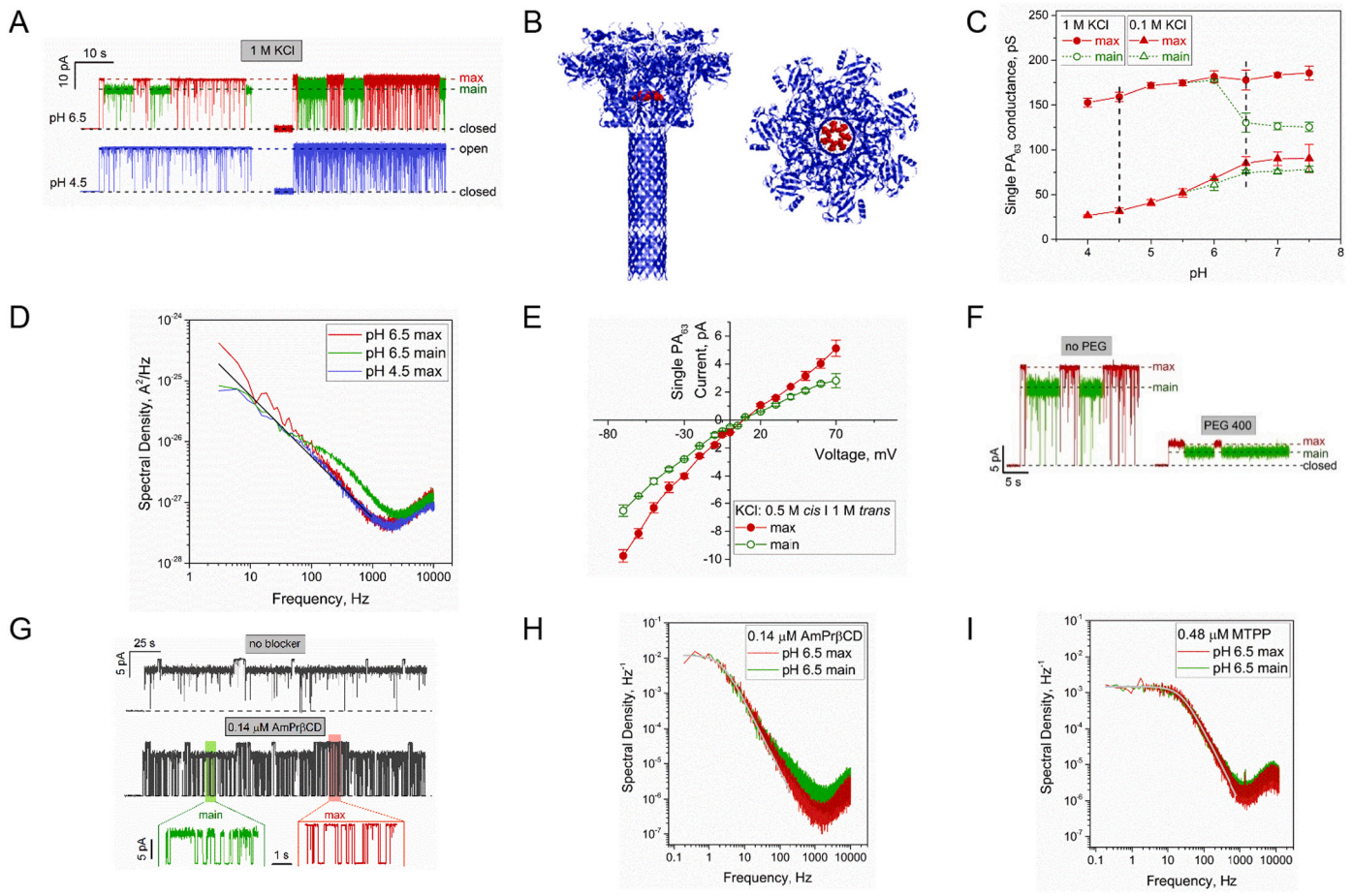

Fig. 4. Two PA_{63} channel conductance states. ***(A)*** Single PA_{63} channel recordings taken at pH 6.5 (*top*) and pH 4.5 (*bottom*), 100 mV, 1 M KCl. ***(B)*** PA_{63} channel, side and top view; 3J9C [5]. The F427 residues are shown as red spheres. ***(C)*** Single PA_{63} channel 'max' state current decreases with lowering solution pH at 100 mV. The effect is more pronounced in 0.1 M KCl compared to 1 M KCl. At high pH values, the "main" conductance states were frequently detected. ***(D)*** Spectral density analysis of the current fluctuation through a single PA_{63} channel at pH 6.5 (both 'max' and 'main') and pH 4.5. At pH 4.5, the current spectra density changes linearly with frequency (slope ≈ −1.0), showing typical characteristics of the so-called 1/*f* process. In the main conductance state at pH 6.5, the spectrum is similar; however, an additional high-frequency component that corresponds to the "noisy" sub-state of the channel is seen. At pH 6.5, spectral density analysis of the completely open state of the channel, collected from several opening events combined into a single fragment, showed an ideal 1/*f* type of behavior (slope ≈ −1.1), similar to the one observed at pH 4.5. ***(E)*** Ion current *vs.* voltage relationship separately taken for the single PA_{63} channels when in the maximum and main conductance states using 0.5 M cis | 1 M trans KCl gradient at pH 6.5. Note the similarity of reversal potentials in both states. ***(F)*** Two states of an open PA_{63} single-channel examined in PEG-free (*left*) and 1.2% (*w*/w) PEG400-containing (*right*) 1 M KCl solutions at pH 6.5 and 100 mV applied voltage. ***(G)*** AmPrβCD channel inhibitor blocks PA_{63} both when the channel is in the 'main' and 'max' states with similar blocked state probabilities. ***(H)*** Power spectral densities of AmPrβCD-induced PA_{63} current fluctuations in the 'main' and 'max' conductance states at frequencies <100 Hz can be fitted by a single Lorentzian. The increase in the current spectral density signal on the main state spectrum at >100 Hz is related to the open channel fluctuation intensity increase. ***(I)*** Power spectral density of MTP-induced PA_{63} current fluctuations in the 'main' and 'max' conductance states are fitted by a single Lorentzian at 50 mV, 1 M KCl, pH 6.5.
Reprinted with permission from ref. [11]. Copyright (2017) John Wiley and Sons and Copyright Clearance Center.

helix compression model of LF translocation trough PA_{63} [60] (see Section 3.4 below for details). In particular, the authors used the Monod, Wyman, and Changeux allostery model fit [61] applied to data on the PA_{63} ion current blockage by LF peptides, however no direct statistical comparison of the peptide/PA_{63} interaction when the channel is in the 'max' and 'main' conductance states was performed (see related discussion in refs [62,63]).

So far there is no direct evidence of any physiological importance of the two-conductance state channel behavior. In our view, the observed conductance pattern likely represents an artifact of the PA_{63} reconstitution attempted under non-physiological conditions. Thus, at pH 6.5 the ratio between the 'max' and 'main' state conductances was significantly greater in 1 M compared to 0.1 M KCl solutions (Fig. 4A), (27 ± 4) % and (11 ± 1) % respectively [11]. Moreover, the difference between the two alternate conductance states, being quite significant at pH 7.5, becomes smaller with lowering pH from 7.4 to 6 and nearly disappears at pH ≤ 5.5 (Fig. 4A, *bottom* and **4C**). At the same time, the monotonic change in the PA_{63} channel conductance with solution pH (Fig. 4C) indicates that at low pH, PA_{63} inserts directly to the 'max' conductance state. Moreover, at pH > 5.5, PA_{63} channels were frequently detected being in their 'max' conductance state without switching to the 'main' state (classified as type I and type II PA_{63} insertions in ref. [58]). Importantly, power density spectra of the current fluctuations at pH 4.5 and pH 6.5 (the "max" state) were nearly identical, showing an ideal 1/*f* behavior (see Section 3.3.3 for details), whereas the power spectrum of the current fluctuation in the 'main' state had an additional high-frequency component (Fig. 4D) [11]. The authors also reported that in 1 M KCl at pH 6.6, the "max" conductance state channels represented ~40% of all the insertion in DPhPC but only ~8% in DPhPS bilayer membranes. Yet, in DPhPS the 'max'/'main' current step was significantly greater compared to DPhPC, representing about 30% of the total conductance. Importantly, PA_{63} selectivity remained nearly the same when the channel current was switching from the 'max' to 'main' conductance states (Fig. 4E). Thus, under the 0.5 M *cis*|1 M *trans* KCl

concentration gradient, the channel had approximately three times higher preference for cations compared to anions in both the 'max' (E_{rev} = 9.1 ± 0.5 mV) and 'main' (E_{rev} = 8.6 ± 0.4 mV) states.

To verify whether the two conductance states represent the structurally distinct conformation of the channel, with dilation taking place at the ϕ-clamp [56], several molecular probes known to modify PA_{63} channel conductance were tested [11]. First, partitioning of a water-soluble polymer, poly-(ethylene glycol) with a molecular weight of 400 Da (PEG400), in the channel lumen was investigated (Fig. 4F) (see Section 3.3.5 for details). Because PEG400 was previously shown to generate the most significant reduction in PA_{63} ion current [64], the authors expected this polymer to be sensitive to the presumptive changes in the channel dimensions. PEG400-induced decrease in the 'max' and 'main' state current, $\frac{I_{PEG400}}{I_{no\ PEG400}}$ = 0.24 ± 0.02 and 0.20 ± 0.01 correspondingly, was hardly detectable (p-value = 0.03). Second, when the 'max' and 'main' states were probed using two efficient cationic aromatic blockers (see Section 3.5 for details), per-6-(3-amino-propylthio)-β-cyclodextrin (AmPrβCD) (Fig. 4G) and methyl-triphenylphosphonium ion (MTP), kinetic parameters of the PA_{63}/blocker interaction, examined using the power spectral density analysis (Fig. 4H and I) were nearly identical. AmPrβCD is known to interact with the Phe427 residue [57] and MTP ion not only was suggested to bind to Phe427 [56] but is also small enough to translocate through the channel [65]. With both AmPrβCD and MTP, the blocker-induced reversible current fluctuations were described as a two-state Markov process, manifested by a Lorentzian shape of the power spectral density (Fig. 4H and I). The PA_{63}/AmPrβCD and PA_{63}/MTP binding reaction k_{on} and k_{off}, when compared in the 'max' and 'main' states, were within the limits of experimental error [11]. Hence, if indeed the 'max' and 'main' switches represent the channel dilation at the ϕ-clamp region, it is unclear why the studied blockers, which are known to interact with the ϕ-clamp residues, are not sensitive to the changes in the region dimensions. Kalu et al. suggested that because at pH < 5.5 the PA_{63} channels are always detected in the 'max' conductance state (also known as type II insertion [58]) and because the channel is evolved to operate in the acidic endosomal environment, at pH ≥ 5.5 it forms but collapses to the more energetically favorable but not fundamentally different structural conformation [11]. There is no evidence that the supposed structural changes take place at the ϕ-clamp region.

3.3.2. PA_{63} voltage gating

Voltage gating was previously described as a fundamental feature of the β-barrel bacterial porins and channel-forming exotoxins in PLMs [66]. The process is manifested by switches in ion current through the channels to non-conductive or low-conductive states; the probability of channel closure increases with an increase in the transmembrane voltage. In PA_{63} channels, the voltage-dependent closures are complete (Fig. 5A) and highly asymmetric, being much more pronounced in *cis*-negative compared to *cis*-positive voltages (Fig. 5B) [39–41,58,67]. Similarly to many other β-barrel transmembrane channels, the PA_{63} voltage gating events are quasireversible; PA_{63} shows a tendency to stay at a non-conductive state for minutes and, occasionally, hours, even when the applied voltage is reduced to zero [58]. Interestingly, the second-long pulses of opposite sign voltages as high as ±250 mV often made the channel reopening possible. The voltage-dependent gating of the cysteine-substituted PA_{63} channels was reported to be stopped by a reaction with a methanethiosulfonate reagent that catalyzes the formation of intersubunit disulfide bonds [68]. The voltage gating in PA_{63} is lipid-dependent (Fig. 5C) [58,69]. The channels were much less sensitive to the applied voltage when reconstituted in DPhPS compared with DPhPC membranes [58], showed comparable voltage gating activity in DOPC, DOPS, and DOPE membranes, and significantly higher voltage sensitivity in DOBMP [69]. Unfortunately, origin and physiological significance of the voltage-dependent PA_{63} closures, more than 30 years after being reported for the first time [39], are still unclear. At this moment, we can only suggest that the high asymmetry in the PA_{63} gating toward the sign of applied voltage can prevent PA_{63} from the LF and EF off-target translocation by keeping the channel closed. The endosomal limiting membrane potential is known to be inside-positive [70,71], favorable for the open PA_{63} channel conformation.

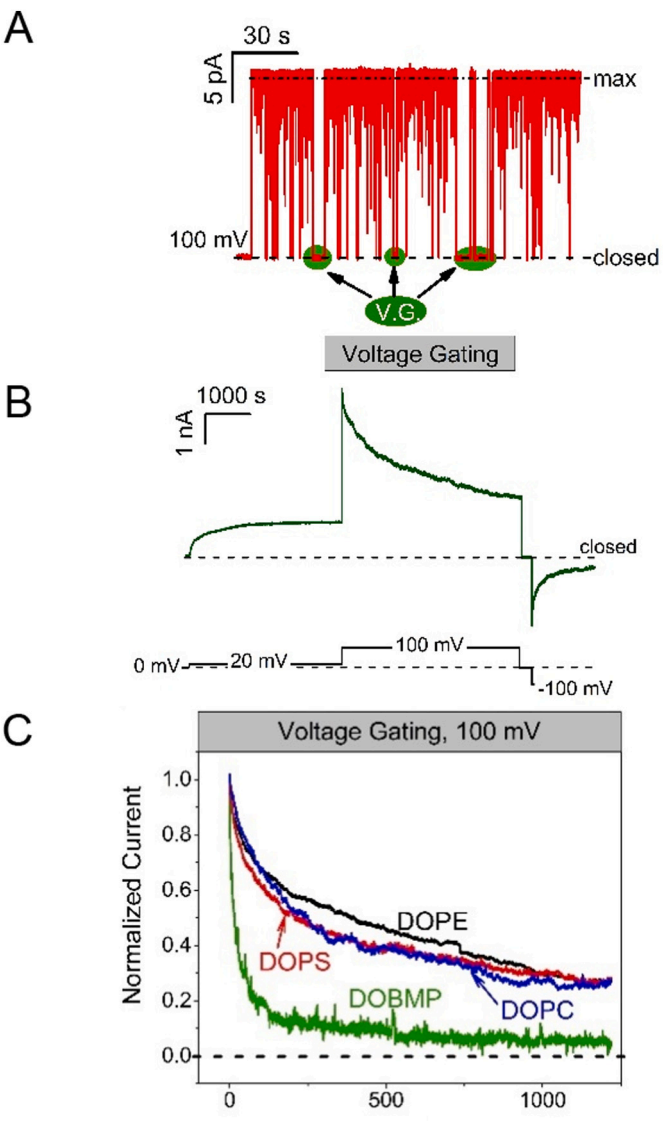

Fig. 5. PA_{63} voltage gating. ***(A)*** The single PA_{63} ion channel current track taken at 100 mV shows reversible voltage gating events (*highlighted in green as V.G.*). ***(B)*** Multichannel ion current recordings showing asymmetry in the channel gating toward the voltage sign. ***(C)*** Difference in PA_{63} voltage gating is nearly indistinguishable in DOPC, DOPE, and DOPS but showed a strong effect in DOBMP bilayers.
Reprinted with permission from ref. [69]. Copyright (2018) Elsevier.

3.3.3. 1/*f* noise in PA_{63} current

Apart from the 'max'/'main' current states switches and voltage-dependent closures, the intricate kinetic behavior of PA_{63} also includes intense voltage-independent current flickering between completely open and closed states (Fig. 6A). In a wide, −20 - +100 mV, range of applied voltages, power spectral density plots [72] of the PA_{63} current fluctuations in the $\log_{10}$-$\log_{10}$ scale, can be fitted by a negative linear dependence (Fig. 6B). The slope of the linear dependences is equal to −1 at frequencies < (100−2000) Hz, which is typical for the so-called 1/*f* noise. In contrast to the voltage gating, the 1/*f* noise events were time-independent and highly reproducible between the individual

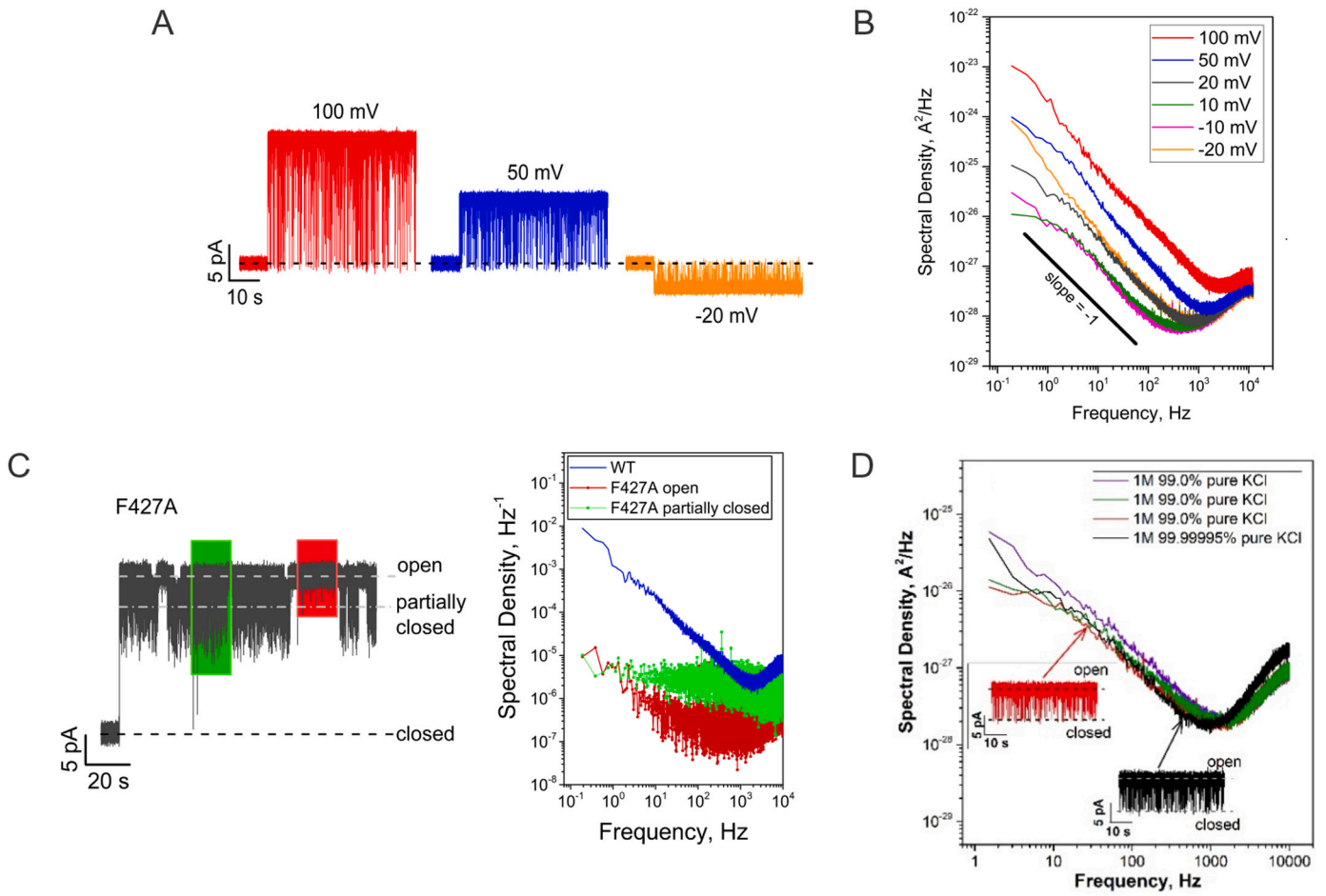

Fig. 6. 1/*f* noise of single PA_{63} channel. ***(A)*** Typical ion current recordings through a single PA_{63} channel, taken at 100, 50, and − 20 mV; 1 M KCl, pH 6.0. ***(B)*** The power spectral densities of PA_{63} 1/*f* noise current fluctuations, when plotted in the log-log scale, have slopes, which are close to −1, when taken at different transmembrane voltages (−20 − +100 mV) at a wide range of frequencies. ***(C)*** Removal of the ϕ-clamp disrupts 1/*f* noise behavior as seen on a typical single PA_{63}-F427A channel recording (*left*) and power density spectra (*right*). ***(D)*** Power spectral densities of single PA_{63} current fluctuations measured in 1 M 99.0% pure (*purple, green, and red spectra*) and 99.99995% pure (*black spectrum*) KCl solutions.
Reprinted with permission from ref. [62]. Copyright (2017) National Academy of Sciences.

channels [62]. The 1/*f* fluctuations in PA_{63} current were observed in a variety of experimental conditions, including different bathing electrolyte composition, concentration, purity, and pH, different lipid composition, in both 'max' and 'main' conductance states, and in octameric and heptameric channels [11,51,58,62,65]. These factors do not have any measurable effect on the kinetic parameters of the 1/*f* fluctuations [73]. Importantly, removal of the ϕ-clamp resulted in complete elimination of the 1/*f* noise behavior in experiments with the PA_{63}-F427A mutant (Fig. 6C) [58], which may indicate that the process itself is generated at the narrow hydrophobic ϕ-clamp region of the channel. It was suggested that the current flickering process can be caused by the presence of "a contaminant small molecule, buffer ion, or peptide" that "momentarily binds and occupies the ϕ-clamp" [59]. However, this hypothesis was ruled out in the experiments where PA_{63} current noise was compared in KCl solutions of different purity; no change in density of the current power spectra was detected (Fig. 6D). It was also suggested that the 1/*f* noise in PA_{63} current occurs as a result of the so-called 'hydrophobic gating' [74] at the ϕ-clamp region [75] with or without stochastic movements of the F427 residues that may temporarily create an impermeable physical barrier for the small ion current [73].

3.3.4. *Solution pH and two distinct patterns of PA_{63} conductance dependence on KCl concentration*

When in the 'max' conductance state, PA_{63} current decreases monotonically with lowering solution pH (Fig. 4C) [11]. This effect, being more pronounced at low salt concentrations, was interpreted as a reversible protonation/deprotonation of the charged residues in PA_{63} lumen. PA_{63} channel current also shows an unusual pH-dependent bathing electrolyte concentration dependence (Fig. 7A). At pH 6.5, both 'max' and 'main' conductance states follow very weak KCl concentration-dependent behavior [40,67]. At pH 4.5, the channel conductance changes linearly with the bathing solution concentration, showing nearly 1:1 dependence on the KCl solution conductivity [11]. These data may indicate that one or several amino acids in PA_{63} lumen change their ionization state with solution pH decrease. Thus, the 1:1 channel conductance/bulk concentration dependence is expected for a neutral, nonselective channel, whereas conductance saturation at low supporting electrolyte concentrations is typical for the protein channels with ionizable residues [76,77]. This is not the case here; PA_{63} demonstrates a strong preference for cations both at low and high KCl, independently of the solution pH (Fig. 7B). Kalu et al. suggested that at pH 6.5, PA_{63} conductance is mainly determined by the distribution of the fixed charges in the channel lumen, most likely by one or several amino acids in proximity to the ϕ-clamp that create ionic-strength-dependent electrical potential attracting cations [11]. At pH 6.5, the

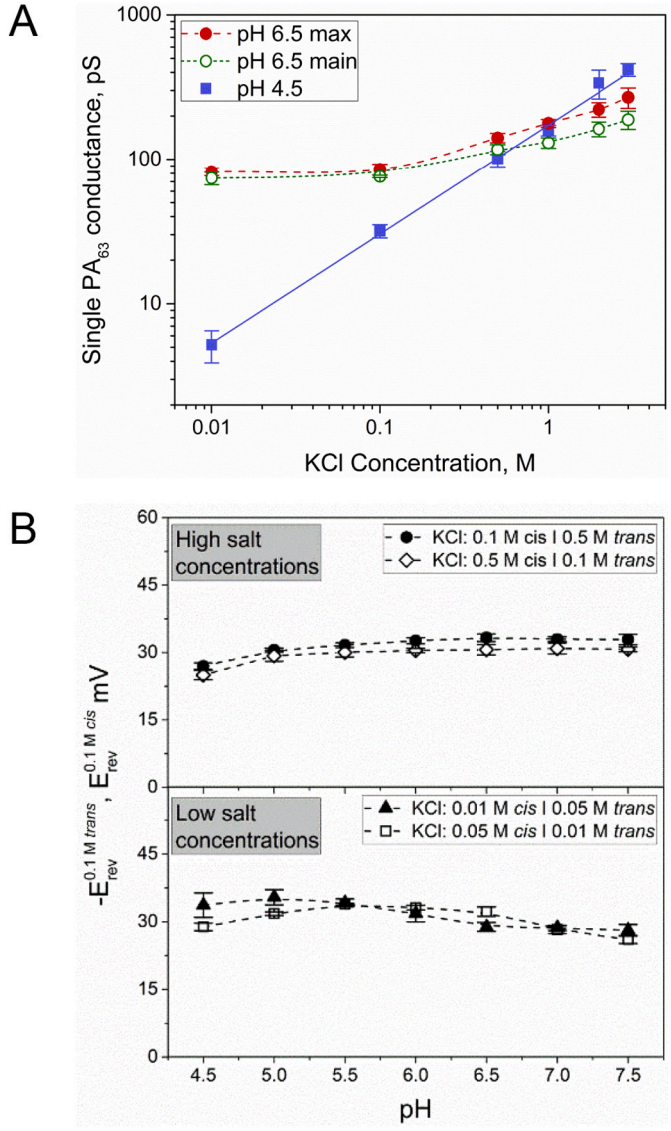

Fig. 7. PA_{63} small ion transport properties. ***(A)*** Single PA_{63} ion current (both in max and *main* states) dependence on bathing KCl concentration is pH-dependent with a weak dependence observed at pH 6.5 and nearly linear change at pH 4.5. ***(B)*** Dependence of PA_{63} E_{rev} on solution pH at high *(top)* and low *(bottom)* concentration gradients.
Reprinted with permission from ref. [11]. Copyright (2017) John Wiley and Sons and Copyright Clearance Center.

cation can interact with the aromatic π-motif of the neutral forms of histidine residues *via* cation-π interactions or bind to anionic glutamic or aspartic acid residues, if their pKs are shifted toward higher numbers. When at pH 4.5 the suggested residues got protonated, PA_{63} conductance at low salt concentration is largely determined by the access resistance of the narrow ϕ-clamp region of the channel. Because the channel selectivity is rather determined by a concerted action of many channel lumen residues, it does not change its pattern in the discussed pH range.

3.3.5. *Effect of PEG on the PA_{63} current conductance*

Another unusual property of the PA_{63} current was reported in a study where poly(ethylene glycol)s were used to size the limiting diameter of the channel (Fig. 8) [64]. The polymer partitioning into ion channels is an informative technique frequently used to estimate the size of the channel lumen, perform single-molecule sensing, and investigate polymer-assisted transport [78,79]. The addition of the nonelectrolyte polymers changes bathing electrolyte conductivity and interferes with ionic flow through channels in a polymer molecular weight-dependent manner. Upon addition of differently sized PEGs (Fig. 8A), PA_{63} channels showed a clear transition between the polymer penetration and exclusion regimes (Fig. 8B) providing the PEG molecular mass cutoff of ~1400 Da [64]. The authors determined the heptameric PA_{63} polymer-accessible aperture diameter being ≤20 Å, mentioning that the PEG-sizing method may overestimate the channel-limiting aperture diameter, provided the PA_{63} permeant PEGs do not transport completely through the limiting aperture of the channel. At the same time, it was demonstrated that small PEGs decreased the channel current to a much greater extent than they decrease the bulk solution conductivity. Thus, the authors had to perform their measurements using 1.2% (*w*/w) PEG concentrations instead of the 15% PEG solutions traditionally used for the ion channel sizing experiments. The suggestion was made that either PEG concentration inside the channel is significantly higher compared to its concentration in the bulk solutions or that the aqueous solution in the PA_{63} lumen is not bulk-like [64]. Thus, the small PEG, added at very small concentrations, can reduce the channel current because water inside the pore is organized differently compared to the bulk or to other channels, such as α-HL. It was also suggested that the channel limiting diameter can be so narrow that a single PEG molecule may nearly block the ion-conducting pathway. Moreover, at 10 mM ≥ concentrations, even the large, supposedly impermeant, PEG decreased the channel conductance (Fig. 8C), independently of the PEG molecular mass. Because the addition of a chemically different polymer, dextran 4900 (Fig. 8C, *insert*) led to a very similar effect, the authors suggested that the conductance decrease is unlikely to be caused by highly specific chemical interactions between the polymers and PA_{63}.

3.4. *PA_{63} translocase activity*

A generally accepted model of LF and EF delivery from the endosomal compartments into the host cell cytosol states that the enzymes are transported through the PA_{63} lumen with the channel playing an active role in their unfolding and translocation [80]. The channel-facilitated translocation model is supported by a number of carefully designed PLM experiments [32,33,56,60,81–91] where roles of the different factors, such as transmembrane voltage and pH gradient on the enzymatic factor translocation rates through the PA_{63}-WT and mutant channels were investigated. Because of the steric constraints imposed by the PA_{63} lumen geometry, LF and EF components must unfold to translocate through the channel [36]. Our viewpoint on the PA_{63} limiting diameter, at the ϕ-clamp region, has changed in 2015, when a heptameric structure of the channel was determined at a 2.9-Å resolution using cryo-EM [5] (Fig. 4B). Prior to that, Finkelstein's group, using measurements on voltage-dependent tetraalkylammonium ion permeation, determined that the limiting diameter of the channel was close to 12 Å [40]. In particular, based on the characteristic residence time *vs.* transmembrane voltage behavior (an increase followed by a steady decline) and independence of the residence time on the side of their addition (*cis* or *trans*), it was demonstrated that ~12 Å tetraheptylammonium ions were translocating through the channel. A very similar cut-off was recently detected using PA_{63} blockers; 7.7 × 10.8-Å MTP ions, but not 15-Å G0-PAMAM dendrimers, were shown to translocate through the channel [65]. The channel sizing experiments using PEGs (Fig. 8) [64], have estimated PA_{63} diameter being close to 20 Å, however, the authors admitted that the value may represent a certain overestimation of the limiting region diameter provided the polymers do not go all the way through the channel (see Section 3.3.5 for details). Nevertheless, the atomic resolution structure of the channel showed the ϕ-clamp region being as narrow as 6 Å [5]. The authors however suggested that considering that the channel is able to translocate the enzymatic components with the side chains of various diameters, it is possible that the ϕ-clamp acts as an elastic sealed 'O-ring' able to change its dimensions and shape to transport its cargo effectively. From then on,

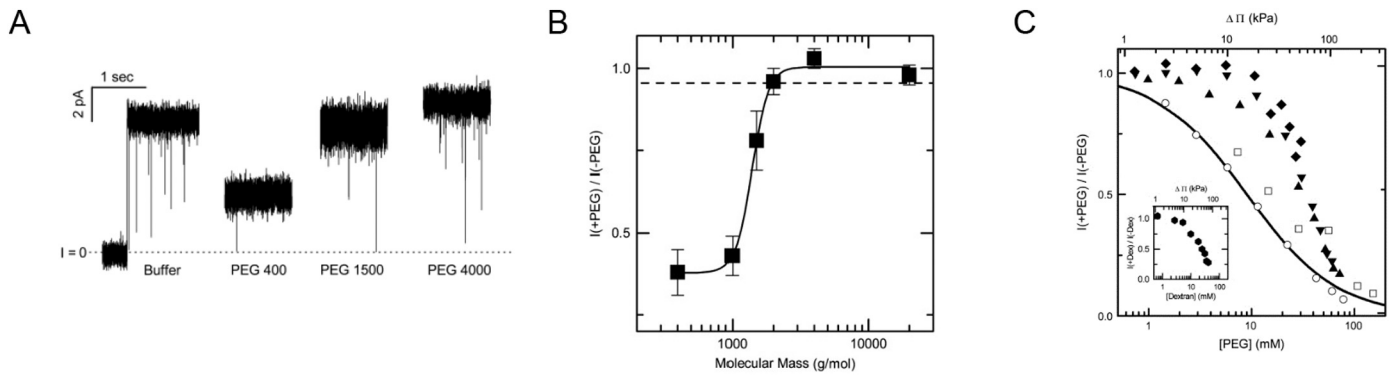

Fig. 8. PA_{63} channel response to PEG addition. ***(A)*** Single PA_{63} channel ion current in 1.2% (w/w) different molecular weight PEG solutions, 0.1 M KCl, pH 6.6, 100 mV. ***(B)*** The effect of PEG molecules of different size on the anthrax toxin channel ionic current. The PEGs with molecular masses <2000 g/mol partitioned into PA_{63} decreasing the current. ***(C)*** Single PA_{63} channel ion current dependence on PEG concentration with PEG400 (*open squares*), PEG1000 (*open circles*), PEG1500 (*solid triangles*), PEG2000 (*solid down triangles*), and PEG4000 (*solid diamonds*). (*Inset*) the effect of dextran4900 on the ion current through the channel.
Reprinted with permission from ref. [64]. Copyright (2008) Biophysical Society.

the idea of the ϕ-clamp flexibility has gained increasing interest [59,75,92,93].

Distancing from the limiting PA_{63} diameter problem, it is important to mention that the anthrax toxin enzymatic components still need to unfold to traverse the channel constrictions sites, ϕ-clamp, and β-barrel stem. The LF and EF unfolding and translocation which starts from their N-terminal domains [32,94], is facilitated by the acidic endosomal environment [95]. Originally, the overall translocation mechanism was described as a 'Brownian ratchet', in which the protein gradient (ΔpH) and, possibly to some degree, electric potential gradient (Δψ) across the endosomal membranes, drive the LF and EF translocation [81,82,84,86,96–98]. A ΔpH appears to be sufficient to drive translocation of LF, EF, and EF_N [29,48,81], while LF_N was shown to translocate under a pure Δψ [33,56,81,83]. The ϕ-clamp, being able to bind and transport cationic and aromatic residues, excludes anionic Asp and Glu residues. According to the model, when the LF and EF's anionic residues got protonated, even momentarily, at the acidic endosomal pH, they can traverse the ϕ-clamp seal and got instantly deprotonated facing the high cytosolic pH environment in the channel vestibule. As a result, the polypeptide chain gets trapped inside the channel, because the deprotonated negatively charged residues are not able to translocate in the opposite direction (reviewed in refs [47,87,99,100]). In addition to the Phe427 ring, Krantz's group has also identified several additional 'peptide clamps' throughout the length of the channel (Fig. 9A), which were shown to catalyze the LF and EF translocation [48,60,83,84]. First, an α-clamp, the substrate docking surface on the top of the cap side of the channel was discovered [48]. Interactions with the α-clamp were shown to be critical to initiate some destabilization in the substrate structure [48]. Second, the charge-clamp formed by the anionic region in the β-barrel stem part of the channel was identified [84]. It was suggested that the charge-clamp repels the deprotonated anionic substrate fragments preventing their retro-translocation [84,98]. According to the suggested model, the α-, ϕ-, and charged-clamps of the channel nonspecifically bind the different segments of translocating natural enzymatic factors and their engineered variants *via* a variety of interactions. The functional clamps were also described as dynamic rather than static binding sites, which, instead of impeding protein translocation, bind and release the translocating chains in a dynamic manner [100].

An interesting method to demonstrate that all the translocation machinery was contained inside the channel was developed by Zhang et al. using multichannel PLM experiments [32,33] and later was significantly advanced by Finkelstein, Collier, and Krantz group members (Fig. 9B). After insertion of several hundred or thousands of PA_{63} channels into PLMs under low, *e.g.*, +20 mV applied voltage and ion current stabilization, the enzymatic components or their variants were

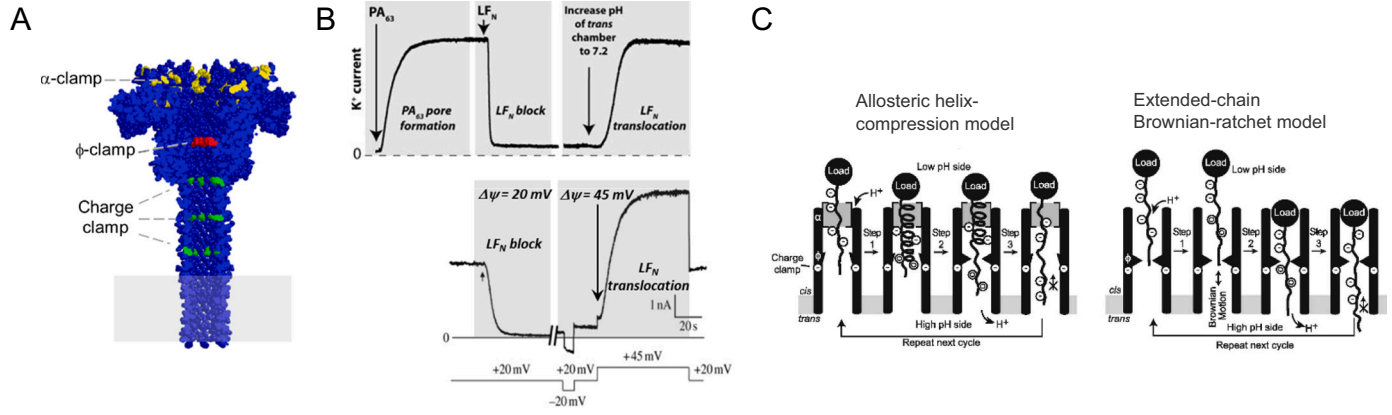

Fig. 9. PA_{63} channel acts as an unfoldase and translocase for its enzymatic substrates and their variants. ***(A)*** Protective antigen channel lumen with the peptide α-clamp, ϕ-clamp, and charge clamp shown, PDB ID 3j9c [5]. ***(B)*** *Top:* Typical PLM PA_{63} multichannel ion current recording showing changes in K^+ current in response to PA_{63} channel reconstitution, LF_N-induced binding and channel block, and ΔpH-induced LF_N translocation at +10 mV [101]. *Bottom:* Changes in K^+ current through a multichannel PLM in response to LF_N-induced binding and change in transmembrane voltage gradient from +20 to 45 mV [87]. ***(C)*** Anthrax toxin channel allosteric helix compression *(left)* and extended-chain Brownian-ratchet *(right)* models [102].
Modified with permission from refs [87,101,102]. Copyright (2006) National Academy of Sciences, (2008) The Royal Society, (2017) Elsevier.

added to the *cis* solution, which resulted in a quick decrease of channel current. The effect was attributed to the binding and entry of enzymatic components inside the PA_{63} channels. After perfusing the unbound enzymatic components, a time-dependent increase in the ion current through the multichannel membrane time was initiated either by creating a pH (Fig. 9B, *top*) or voltage (Fig. 9B, *bottom*) gradient across the membrane [32,33,56,89]. The effect was interpreted as the channel-mediated protein translocation. Even though this conclusion is not absolute, it seems persuasive, because the current recovery rate, measured as the time for half of the protein to translocate, $t_{1/2}$, correlated with cytotoxicity of the anthrax toxin complexes, when different PA_{63} mutants and LF and EF variants were investigated. The translocation kinetics of the LF and EF constructs and even their shorter LF_N and EF_N fragments is complex; the S-shaped kinetics of the current recovery likely is a reflection of a multistep translocation mechanism [33]. Note, that the S-shaped kinetics was preserved even with only one LF_N bound to the channel, which was driven by $\Delta\psi$ on a timescale of seconds [89].

In the "Electrophysiology of Unconventional Channels and Pores" book chapter dedicated to the PA_{63} channel, Bryan Krantz provided an excellent summary of the existing anthrax toxin translocation models [100] comparing a barrier-limited [82,98] and a barrier-less drift-diffusion [89] translocation models. The author suggests that the translocation is universally barrier limited [100] with unfolding being a major limiting barrier at voltages <50 mV [82,98]. At larger voltages, translocation is limited by the unfolded chain movement across the channel [82]. The S-shaped kinetics is preserved because the translocating unfolded chain needs to cross many barriers of equivalent height in consecutive order. In the book chapter, Krantz also compares the charge-state Brownian ratchet and helix-compaction models of the ΔpH-driven translocation (Fig. 9C) [100]. To explain the physical forces needed to move the substrate protein under the ΔpH across a highly cation-selective PA_{63} [39], the Brownian ratchet model suggests protonation, probably short-lived, of the substrate Asp and Glu residues under the low pH conditions in the *cis* side of the bilayer chamber or inside the endosomal compartments [81]. The protein chain then moves across the cation-selective region due to Brownian motion and, after passing the major anion repulsive residues, gets deprotonated facing the high pH site of the membrane. The negatively charged chain is not repelled from the anionic PA_{63} regions the protein fragments have passed. As a result, the transmembrane pH gradient acts as a driving force preventing the protein retro-translocation. Pointing to some deficiencies of the original model [81], Krantz and colleagues suggested the two-phased force-transduction mechanism [60,84,98,100], with the first phase being a proton-binding step occurring in a force-generating power stroke manner to unfold the protein and the second phase revealing the charge-state Brownian ratchet features [103,104]. To describe the force transduction mechanics, two different views on the translocating polypeptide chain conformation were considered [100], the 'extended chain model' [90], where the substrate chain is supposed to remain in a single conformation, and the 'helix compaction model' [60], where the translocating chain gets over α-helical and extended conformations along its length in multiple ongoing steps [100]. Considering the large protein translocation, PA_{63} was also suggested to dynamically operate between several states with different levels of dilation [59,92], in particular, the ϕ-clamp region was reported to change its dimensions to accommodate the different fragments of the substrate chain [5,93]. Recently, Machen et al. reported two (3.1 and 3.2 Å) cryo-EM snapshot of the PA_{63} channel caught in the act of translocating LF_N [105]. The authors show that LF_N unfolding starts near the α-clamp and then, after translocating through the ϕ-clamp, LF_N begins refolding in the charge clamp. While there were no multiple distinct channel states captured, smeared density around the ϕ-clamps showed that it is likely dynamically moving up and down along the pore axis.

3.5. Inhibiting the PA_{63} translocation channel

PA_{63} is not only an amazing tool to investigate different aspects of ion channel structure-function mechanisms but also a central component of the tripartite anthrax exotoxin believed to be actively involved in LF and EF translocation into the cytosol. The translocation channel formed by PA_{63} is an attractive and well-defined drug design target to explore (reviewed in refs. [106–109]) that can potentially be inhibited at the various stages of the toxin uptake (Fig. 2). Thus, the future antitoxins may target monomeric PA_{83} receptor binding, its cleavage by extracellular furin to PA_{63}, PA_{63} oligomerization to a prepore, LF/ and EF/prepore interaction, PA_{63} prepore-to-pore conversion, and the PA_{63} pore translocation pathway (reviewed in ref. [107]). For the purpose of this review, we will consider only the last step describing the recent attempts to inhibit the anthrax toxin by blocking PA_{63}-mediated translocation of LF and EF components (Fig. 10A).

There were two different types of approaches designed to disrupt the PA_{63} channel's translocation pathway. First, dominant-negative mutants of PA that co-assemble with the PA_{63}-WT protein and constrain its ability to transport the enzymatic components have been proposed [110–113]. Importantly, a single dominant-negative subunit containing the key amino acid mutations, above all Phe427 mutated to any residue except Trp, Tyr or Leu, was sufficient to disrupt the PA_{63} heptamer translocation function [114].

Second, a significant number of structurally different non-peptide compounds directly obstructing the PA_{63} channel conductive pathway were designed and tested. PA_{63} channels are cation-selective (Figs. 4E and 7B) [85]. To the best of our knowledge, all tested positively-charged ligands (see Fig. 10B for several representative examples) reversibly blocked K^+ current through the channel at a wide (nM-mM) range of their *in vitro* concentrations in PLMs [40–42,56–58,65,67,115–125]. The inhibitors were added to the endosomal cap-side of the channel. This observation suggests the availability of anionic binding sites in the PA_{63} vestibule for the cationic ligands to bind. Yet, the most hydrophobic of those compounds, primarily those possessing aromatic moieties, were among the most effective anthrax toxin channel inhibitors [56,57,65]. Thus, the cationic ligands carrying several aromatic rings were the ones that had a low nM range of binding affinity to PA_{63} [56]. A significant decrease in the inhibitory concentrations of the cationic blockers was achieved when multiple copies of the positively charged ligands were attached to a centrosymmetric β-cyclodextrin scaffold *via* thiohydrocarbon linkers [115,126,127]. Multivalency is one of the most promising recent approaches to convert the weak non-covalent monovalent interactions into a strong binding by creating multiple points of contact between multivalent ligands and their binding sites [128]. The initial idea behind the design of these compounds was to benefit not only from their multivalency but also from symmetry match between the heptameric structure of the channel and 7-fold symmetry of the cyclodextrins. The expectation was that the attached cationic ligands would concurrently occupy matching symmetrical binding sites of the target channel. Yet even with these multivalent [109] cationic inhibitors, the introduction of an aromatic moiety, *e.g.* a phenyl group as a part of the linker groups (Fig. 10B, *bottom*), resulted in an increase in blocker activity, primarily due to the binding reaction off-time increase [57]. Remarkably, affinity of all the cationic blockers toward the channel was dramatically reduced when a single F427A mutation was introduced [56]. Inhibitory activity of another group of multivalent cationic substrates, which were based on a completely different, poly(amidoamine) PAMAM dendrimer scaffold was also investigated [109,122,123]. Dendrimers are repeatedly branched starburst-shaped polymers with all bonds emanating from a central core [129,130]. Each consecutive growth step represents a new 'generation' (G0 – G10) of dendrimers with an increased diameter and doubled number of functional groups. In PLMs, all but the smallest G0 dendrimers were reported to inhibit PA_{63} channels at low-nM concentrations. Interestingly, not only the 15–45-Å G0 - G4 dendrimers but also 97-Å G8 and 135-Å G10 were effectively

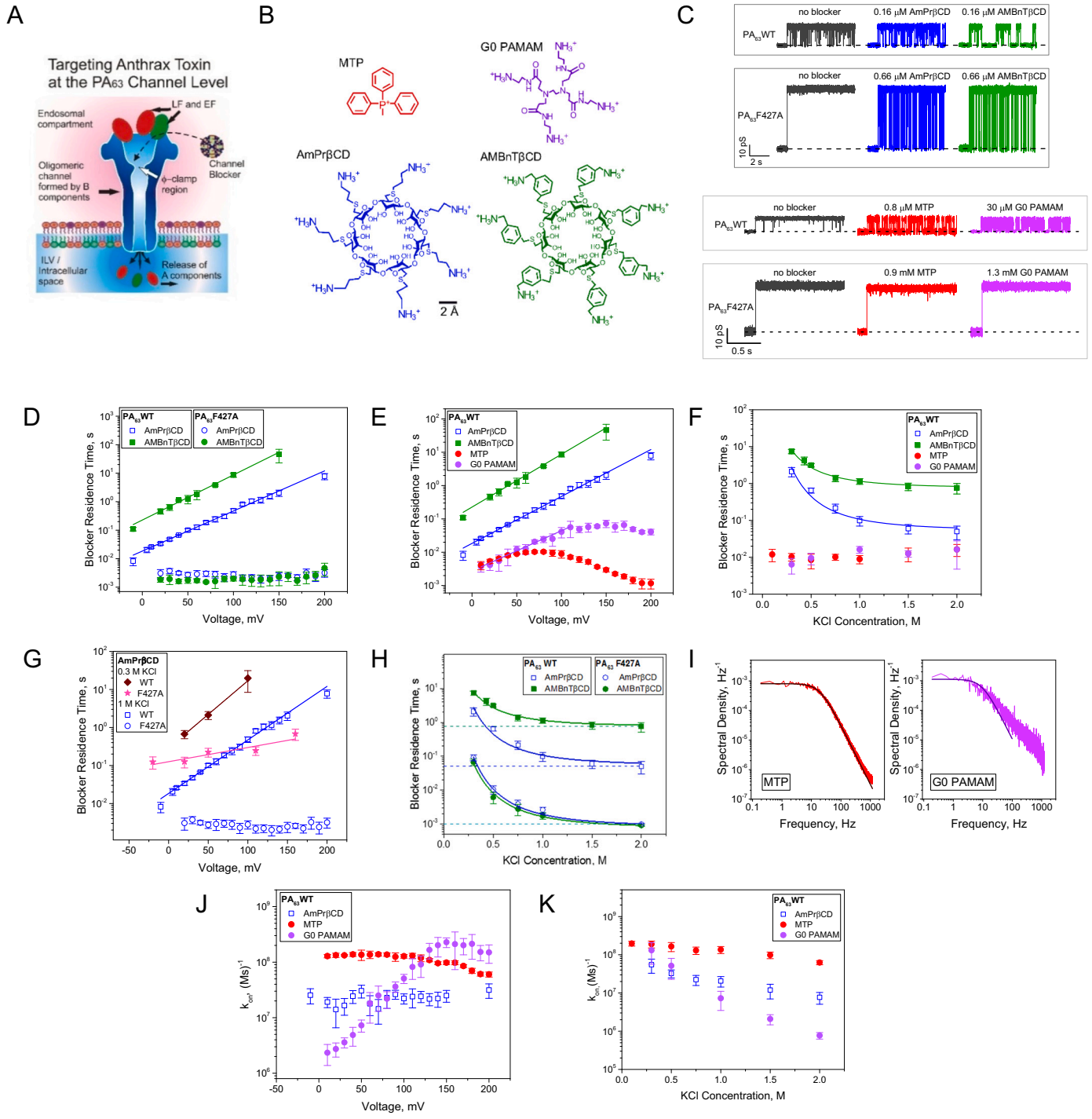

Fig. 10. Inhibition of PA_{63} channel with cationic blockers. ***(A)*** Illustration of the idea: a cationic blocker as an effective inhibitor of PA_{63}. ***(B)*** Schematic representation of MTP, G0-PAMAM, AmPrβCD, AMBnTβCD cationic blockers. ***(C)*** Modulation of single PA_{63}-WT and PA_{63}-F427A currents by *cis* addition of AmPrβCD and AMBnTβCD (*top two panels*) and MTP and G0-PAMAM (*bottom two panels*) at 50 mV transmembrane voltage, 1 M KCl, pH 6. ***(D)*** Residence times of AmPrβCD and AMBnTβCD binding to PA_{63}-WT and PA_{63}-F427A. ***(E)*** Residence times of MTP and G0-PAMAM as a function of voltage show a multiphasic behavior, different from the single-exponential increase observed for AmPrβCD and AMBnTβCD. ***(F)*** Residence times of MTP and G0-PAMAM are salt concentrations independent (50 mV), which is distinct from the effect observed with AmPrβCD and AMBnTβCD. ***(G)*** The residence time of AmPrβCD binding to PA_{63}-WT shows exponential dependence on voltage both in 1 M and 0.3 M KCl solutions. In contrast, there is no (1 M KCl) or little (0.3 M KCl) dependence of the AmPrβCD/PA_{63}-F427A binding reaction residence time on the applied voltage. ***(H)*** Residence times of AmPrβCD and AMBnTβCD binding reactions as functions of bulk KCl concentration show different degrees of salt dependence for PA_{63}-WT (*weaker*) and PA_{63}-F427A (*stronger*). The dwell times of the AmPrβCD and AMBnTβCD bindings to PA_{63}-F427A are indistinguishable (*circles*) but differ in the case of PA_{63}-WT (*squares*). The dashed lines indicated salt concentration-independent components of the blocker interaction. ***(I)*** Power spectral densities of the MTP (*left*) and G0-PAMAM-induced (*right*) fluctuations taken with PA_{63}-WT. While the MTP-induced spectrum can be fitted by an ideal single Lorentzian at a wide, 0.2–1000 Hz, range of frequencies, the G0-PAMAM spectrum has an additional component at $f > 100$ Hz. ***(J)*** The on-rate constant of AmPrβCD/PA_{63}-WT binding reaction is voltage-independent; the MTP on-rate shows only a moderate decrease; the G0-PAMAM binding reaction on-rate is voltage-dependent, with the values expanding over two orders of magnitudes. ***(K)*** The on-rate constant of the blocker/PA_{63}-WT binding reaction decreases with the bulk KCl

concentration increase.
Reprinted with permission from ref. [65]. Copyright (2019) Elsevier.

inhibiting PA_{63} [122]. The authors explained the G8 and G10 PAMAM dendrimer activity by their conformational flexibility.

Recently, to understand the physical basis of PA_{63} selectivity for a particular ligand Momben Abolfath et al. investigated several structurally distinct cationic blockers, namely per-6-S-(3-amino) propyl-β-cyclodextrin (AmPrβCD), per-6-S-(3-aminomethyl) benzyl-α-cyclodextrin (AMBnTαCD), per-6-S-(3-aminomethyl) benzyl-β-cyclodextrin (AMBnTβCD), per-6-S-(3-aminomethyl) benzyl-γ-cyclodextrin (AMBnTγCD), methyltriphenylphosphonium ion (MTP), and G0 poly (amidoamine) dendrimer (G0-PAMAM) against both heptameric and octameric PA_{63} variants and PA_{63}-F427A mutant (Fig. 10B and C) [65]. The authors showed that the cationic blockers interact with PA_{63} through a combination of forces instead of binding exclusively to the anionic residues or to the F427. The ϕ-clamp removal weakened the β-cyclodextrin (βCD) interaction with the channel by ~2 kcal/mol for AmPrβCD and 3 kcal/mol for AMBnTβCD and eliminated the MTP and G0-PAMAM binding (Fig. 10C and D). Moreover, while with PA_{63}-WT AmPrβCD and AMBnTβCD residence times followed exponentiation dependence as a function of voltage, the blocker interaction with PA_{63}-F427A was voltage-independent (Fig. 10D). At the same time, the lifetimes of MTP and G0-PAMAM interaction with PA_{63}-WT (Fig. 10C, *bottom*) were voltage-dependent (Fig. 10E) pointing at the ϕ-claim as the major binding site responsible for the voltage-dependent component of the blocker binding. The detected crossover behavior (Fig. 10E) of residence times is often associated with the translocating particles, which are dragged through channels by high voltage displaying a reduction in t_{res}. The observed voltage dependence indicates the blocker charge interaction with the applied transmembrane field [131], pointing out the electrostatic nature of the blocker binding. It was suggested [56,65] that the cationic compounds bind to the phenylalanines of the ϕ-clamp *via* cation-π interactions [132,133], which are the stabilizing interaction of a cation with an electron-rich π system. At the same time, AmPrβCD/PA_{63} and AMBnTβCD/PA_{63} interactions are salt concentration-dependent (Fig. 10F) [57,58,65], suggesting the additional contribution of Coulomb interactions between the amino groups carried by the blockers and negatively charged residues in the channel lumen to the binding process. This effect represents the major force contributing to the cyclodextrin/PA_{63}-F427A binding reaction off-rate [65]. While the salt concentration sensitivity of the Coulomb component of 7 + βCD binding to PA_{63} is straightforward: increase in salt concentration results in the screening of the charge-charge interactions, the salt concentration independence of the cation-π component as is seen with the MTP and G0-PAMAM blocker binding, is interesting. Both the MTP/PA_{63} and G0-PAMAM/PA_{63} binding reaction off-rates were salt concentration-independent (Fig. 10F) and both blockers showed no binding activity toward PA_{63}-F427A (Fig. 10C), which indicates the absence of the Coulomb interaction contribution to the free energy of these blockers binding. While the electrostatic component of the cation-π interactions can be substantial [134], in the system under discussion it takes place at the narrow hydrophobic ϕ-clamp region of the channel. The blocker cationic moieties must dehydrate to enter the region. In addition, because of the high cation selectivity of PA_{63}, anions are highly unlikely to enter the ϕ-clamp. Therefore, we cannot rule out the possibility that in the confined hydrophobic ϕ-clamp environment, the cation-π binding reaction does not obey the rules of simple electrostatics.

It is interesting that only the supposed cation-π component of the βCD binding was voltage sensitive, whereas the Coulomb component had only a subtle effect at low, 0.3 M KCl concentrations (Fig. 10G). To interpret this finding, the authors applied Tikhonov and Magazanik's approach [135] developed as an extension of the classical Woodhull model [131] to take into account an asymmetry in the location of the permeation barrier. The effect of applied voltage on the residence time of a charged blocker has been traditionally described in the framework of the Woodhull model, which applies a two-barrier model to describe the blocker particle binding and transport through the membrane field [131]. Both the on- and off-rates of the binding reaction are assumed to have an identical dependence on the applied transmembrane potential. Tikhonov and Magazanik suggested a modification of this model, which allows for both a barrier and a minimum to change differently with voltage, where δ_b and δ_m are fractions of the membrane field, which respectively correspond to the location of the barrier and the minimum. With the non-translocating blockers, such as βCDs, two extreme scenarios exist. When $\delta_b \approx \delta_m$, only the binding reaction on-rate is voltage-dependent. Alternatively, when $\delta_b \approx 0$, only the off-rate is voltage-dependent. Note that the Woodhull model is developed for $\delta_b \approx 0.5\delta_m$ [131]. Using this approach, Momben Abolfath et al. suggested that the Coulomb component of the 7 + βCD/PA_{63}-F427A interaction takes place under the $\delta_b \approx \delta_m$ conditions when fractions of the membrane field corresponding to a barrier and a minimum are nearly identical. As a result, with PA_{63}-F427A, when only the Coulomb component of the interaction remains, the on-rate is voltage-dependent whereas no (in 1 M KCl) or little (0.3 M KCl) off-time dependence on the applied voltage is detected (Fig. 10G). In the case of 7 + βCD/PA_{63}-WT binding reaction, $\delta_b \approx 0$, therefore the off-rate of the suggested cation-π interaction is voltage-dependent but the on-rate is voltage-independent.

The 7 + βCD binding was also enhanced by introduction of aromatic groups [56], in particular with replacing AmPrβCD by AMBnTβCD (Fig. 10B-F) [57,65,125]. The observed difference in the off-time between these blockers was lost in PA_{63}-F427A (Fig. 10H). The effect could be due to aromatic group π-π interaction with F427 or formation of hydrophobic contacts, which increase the binding affinity of the aromatic blockers. The authors also claimed that in addition to the suggested cation-π interaction, blocker binding to PA_{63} can include a variety of intermolecular forces, such as hydrophobic, π-π (stacking or T), CH-π, ion-dipole, dipole-dipole, and hydrogen bond interaction [65]. In the case of chemically distinct cationic MTP and G0-PAMAM binding, these forces are expected to be quite different. It is suggested that four-positively charged hydrophilic G0-PAMAM mostly binds to the ϕ-clamp region *via* cation-π interactions, while being stabilized by hydrogen bond interaction with the polar residues in the PA_{63} lumen. G0-PAMAM dendrimers may also interact with the channel's negative charges *via* Coulomb interaction, most likely represented by a fast independent process at $f > 100$ Hz (Fig. 10I). In contrast, the hydrophobic MTP, which carried three aromatic moieties and a single positive charge, has only one hydrogen bond acceptor and no hydrogen bond donors. Therefore, with this blocker, the hydrophobic or π-π interaction may predominate.

The on-rates of the AmPrβCD/PA_{63}-WT and AMBnTβCD/PA_{63}-WT blocker associated reactions were practically voltage-independent, which corresponded to the described $\delta_b \approx 0$ conditions [65]. Considering the wide *cis*-opening PA_{63} vestibule and its complementary negative charge, the authors suggested the barrier-free transition of the blockers to the binding site. Yet, with PA_{63}-F427A the on-rate of the remaining Coulomb component of the 7 + βCD binding shows some weak voltage dependence, probably due to a change in the voltage drop profile along the channel with the ϕ-clamp [65]. Interestingly, the MTP binding association rate constant voltage dependence was similar to that observed with 7 + βCDs with only a slight decrease at high voltages related to the voltage-driven blocker permeation (Fig. 10J). At the same time, applied transmembrane field significantly facilitated the G0-PAMAM dendrimer delivery to the binding site, which might be due to increasing flexibility of the G0-PAMAM dendrimer. The association reaction rate constant was found to be salt concentration-dependent with all the studied blockers (Fig. 10K) changing in the following

order: MTP < AmPrβCD < G0-PAMAM. The authors describe the observed effect by screening the blocker positive charges with the counterions at a high salt concentration as well as screening the surface charge of the negatively charged PA_{63} lumen, which decreases the attraction of the blockers to the channel changing their ability to reach the blockage site. Not surprisingly, the described effect was stronger for the most hydrophilic G0-PAMAM blocker.

Finally, in the current system the original 7-fold symmetric blocker against the heptameric channel symmetry match idea [115] has faced an interesting new development. The efficiency of both 7-fold symmetric 7 + βCD and 8-symmetric 8 + γCD against both the PA_{63}-WT heptamers and PA_{63}-(D512K + K245G-R252N) octamers [51] was comparable [65,119]. The sixfold symmetric 6 + αCD blockers binding was significantly weakened. Commenting on the universality of the 7 + βCD and 8 + γCD, which can inhibit interchangeably $(PA_{63})_7$ and $(PA_{63})_8$ variants, the authors suggested that their original strict symmetry match requirement needs to be facilitated [65].

3.6. PA_{63} lipid-dependent properties

The PLM study on the anthrax toxin translocation is one of the most outstanding success stories of channel-mediated protein transport [100]. Yet, the technical details of these model experiments represent an essential simplification of the natural toxin pathway mechanism. One of the examples of such a simplification is the fact that the anthrax toxin translocation experiments were performed exclusively using the synthetic non-mammalian DPhPC membranes. This branched-chain lamellar lipid is commonly used in model PLM experiments due to its high chemical and physical stability and low water and ion permeability [136–138]. At the same time, lipids with the branched hydrocarbon chains are detected in archaebacterial membranes, which are tuned to provide a selective barrier against the harmful environment of hot springs, salt lakes, and extreme acidic and alkaline surrounding [139,140]. Archaebacterial membrane lipid structural and physicochemical properties can be quite different from those of mammalian membrane lipids. In addition, the mammalian membrane lipid composition varies at different stages of the anthrax toxin internalization, *e.g.*, intraluminal vesicle membranes contain ~70% of anionic bis(monoacylglycerol) phosphate lipid (BMP). The anthrax toxin channel was suggested to insert into the endosomal intraluminal vesicle membranes transporting LF inside the vesicles [37].

Recently, using PLM measurements and all-atom molecular

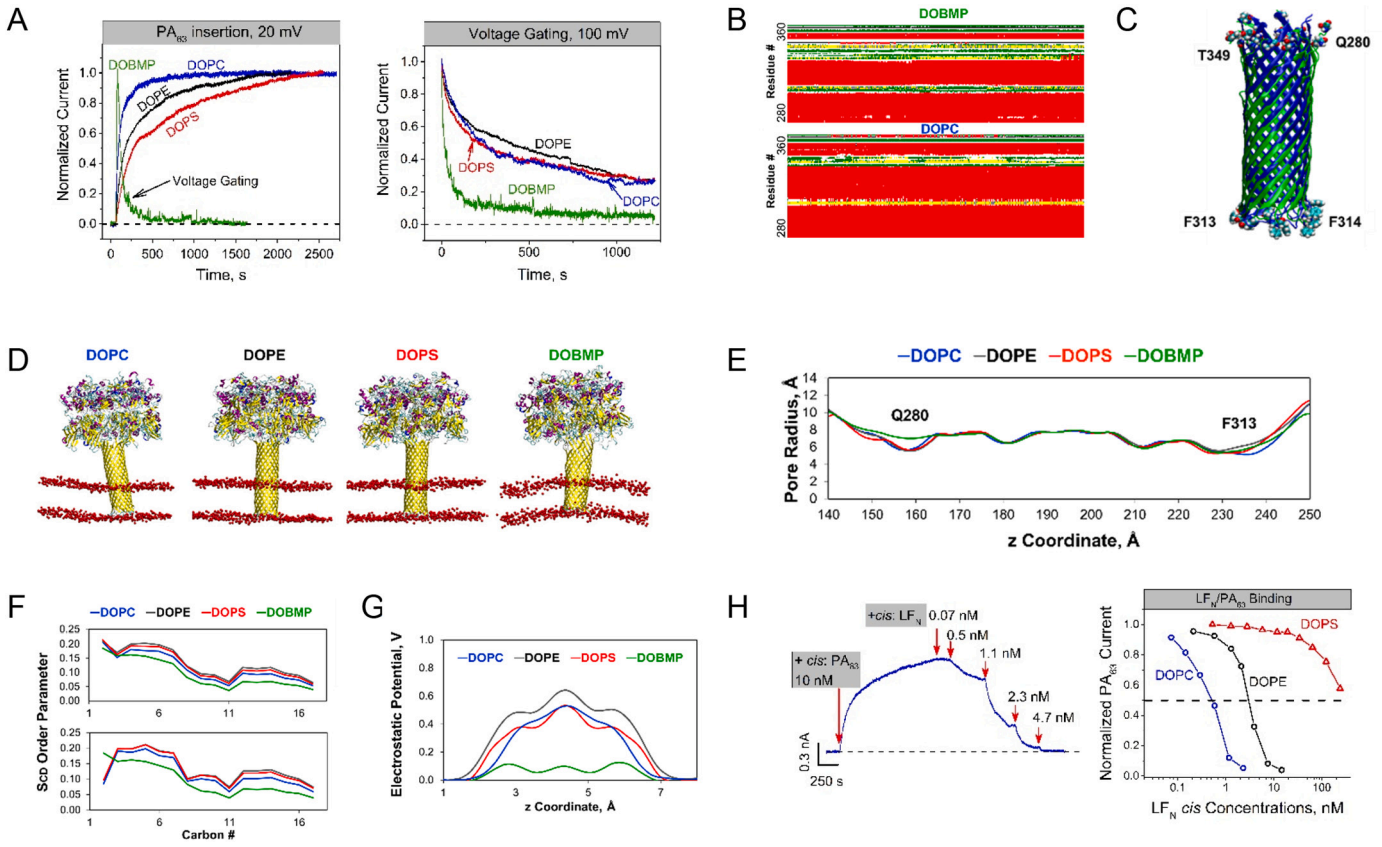

Fig. 11. Influence of membrane lipids on PA_{63} channel properties. ***(A)*** PA_{63} formation rate (*left*) and voltage gating (*right*) are lipid dependent. While the channel formation rate is high in DOBMP, the voltage gating was very strong leading to a quick closure of the channels. The curves were taken in 0.1 M KCl at pH 5.5, under 20 mV applied voltage and normalized by dividing by the maximum current. ***(B)*** Secondary structure comparison for residues 280–350 of a single monomer in the last 50 ns of DOBMP (*top*) and DOPC (*bottom*) trajectories. Coil (*white*), β-sheet (*red*), β-bridge (*black*), bend (*green*), turn (*yellow*), α-helix (*blue*), 3-helix (*gray*). ***(C)*** Structural alignment of the final frames for the DOPC and DOBMP trajectories, respectively highlighted in blue and green. The highlighted residues were selected to illustrate the differences in the conformations of residues with high RMSF values *versus* residues with low RMSF. (***D***) Final snapshot of PA_{63} simulations in DOPC, DOPE, DOPS, and DOBMP. ***(E)*** Mean values of the channel profile in all four lipids as calculated by the HOLE software for the last 100 ns of each of the trajectories. ***(F)*** Average SCD order parameters of the sn1 (*top*) and sn2 acyl (*bottom*) chains (sn1′ for DOBMP) in each of the four simulated bilayers. ***(G)*** Electrostatic potential of the simulated bilayers with the inserted all-atom model of PA_{63}. ***(H)*** *Left:* A typical PA_{63} multichannel LF_N titration experiment. The shown recording was taken in 0.1 M KCl at pH 5.5 in DPhPC membrane; time resolution is 1 s. *Right:* In DOPC, DOPE, DOPS series, the LF_N/PA_{63} binding reaction is significantly affected by lipid nature, with IC_{50} changing as IC_{50} (DOPC) < IC_{50} (DOPE) ≪ IC_{50} (DOPS). In DOPS, IC_{50} could not be reached as increasing concentrations of LF_N over 100 nM resulted in membrane instability and rupture.
Reprinted with permission from ref. [69]. Copyright (2018) Elsevier.

dynamics simulations, it was shown that the anthrax toxin channel properties can be significantly influenced by different membrane lipids, including BMP (Fig. 11) [69]. In particular, PA_{63} channel-forming activity and structural dynamics were shown to be lipid dependent. The channel insertion rate was ~6.5 times and ~ 3 times lower in negatively charged 1,2-dioleoyl-sn-glycero-3-phospho-L-serine, DOPS, and non-lamelar 1,2-dioleoyl-sn-glycero-3-phosphoethanolamine, DOPE, membranes compared to zwitterionic 1,2-dioleoyl-sn-glycero-3-phosphocholine, DOPC. Remarkably, the highest insertion rate was detected in bis (monooleoylglycero)phosphate (S, R isomer), DOBMP, (~1.7 times higher than in DOPC), which is a negatively charged lipid with an unusual sn-1:sn-1′ stereoconfiguration (Fig. 11A). Despite the high rate of insertion, PA_{63} channels reconstituted into DOBMP membranes were unstable, quickly undergoing through the voltage-dependent closures (Fig. 11B, *left*), observed even at 20 mV (Fig. 11A, *right*). Moreover, MD simulations revealed distinct conformational properties of the PA_{63} channels reconstituted in DOBMP (Fig. 11B-D). In particular, the protein SASA profile showed a decrease in the average solvent accessible area of PA_{63} in DOBMP compared to DOPC, DOPE, and DOPS lipids (Fig. 11B). At the same time, the average solvent-accessible areas of several specific residues along the pore lumen (F313 and F314) and the globular regions (K213, N209, N537, N570, and E650) were increased. In DOBMP, the secondary structure of sections of the channel β strands located between residues 280–350 was found to be perturbed near the globular region, which leads to an about 10% loss of the total β-strand content (Fig. 11B) and different conformation of the channel compared to all other lipids (Fig. 11C). At residues 280–350, the channel radius was ~2.4 Å larger in DOBMP compared to the other lipids (Fig. 11E). At the same time, the DOBMP membrane thickness was also somewhat lower, ~35 Å compared to 39–40 Å, which may explain the detected increase in PA_{63} channel formation rate. When the local carbon-deuterium order parameters (S_{CD}) were computed to get a distinct 7-fold axis ordering pattern of the lipids affected by PA_{63}, DOBMP had lower S_{CD} order parameters values than those determined for DOPC, DOPE, and DOPS and a unique form (Fig. 11F). The electrostatic membrane potential computed for each of the four simulated systems showed significantly lower values and a distinct profile for DOBMP (Fig. 11G).

In addition to the insertion rate and voltage gating, PA_{63} small ion transport characteristics were also lipid dependent [69]. However, the effect was mostly determined by the lipid headgroup charge. Thus, in negatively charged DPhPS, DOPS, and DOBMP bilayers, single PA_{63} channel conductance was (20–25) % higher compared to DPhPC, DOPC, and DOPE. However, the cation/anion permeability ratios were shown to be (25–60) % lower in the anionic compared to zwitterionic lipids. Remarkably, PA_{63} selectivity for cations measured in DOBMP ($\frac{P_{K^+}}{P_{Cl^-}} = 7.5 \pm 0.2$) was more than twice as low as in DOPC ($\frac{P_{K^+}}{P_{Cl^-}} = 17.4 \pm 2.8$) (KCl: 0.1 M *cis*|1 M *trans* gradient at pH 5.5).

Another finding, which requires clarification is related to a significant decrease in PA_{63}/LF_N interaction strength in negatively-charged DPhPS and DOPS bilayers (Fig. 11H) [69]. Unfortunately, the strong voltage gating made it impossible to perform similar experiments in DOBMP. The most intriguing detail of the observed ≥100 times increase in IC_{50} values of LF_N binding in DOPS compared to DOPC is related to the fact that the initial binding occurs at the α-clamp cap region of the channel located >100 Å above the membrane surface and therefore the lipid head group charges. The mechanism of the observed effect is currently unclear. The authors suggested that it can be related to the conformational differences in PA_{63} channel structure in different lipid membrane or interaction of LF_N with lipid bilayers leading to the bulk LF_N concentration depletion. While the currently accepted anthrax toxin internalization model does not include any data on membrane activity of the enzymatic factors, there were several studies that reported such an effect [141–144]. Considering that during the natural internalization process, the enzymatic components interact with the membrane receptor-bound PA_{63} prepores, not the channels, the physiological importance of the observed effect remains to be determined.

3.7. PA_{63} as a tumor-targeting agent

Bacterial exotoxins are naturally cytotoxic, which opens numerous possibilities for targeted therapies [145]. The next-generation strategies of the anticancer drug discovery focus on the agents designed to selectively target the unique features of malignant cells, such as specific tumor antigens, carbohydrate structures, growth factor receptors, or cancer-specific proteases [146]. The anthrax toxin, which is composed of three separate proteins that can be tuned independently to target cancer cells, is an excellent candidate for the targeted toxin design (reviewed in ref. [147]). The *Bacillus anthracis* infections are very uncommon and only a very limited group of people is currently required to receive the anthrax vaccine; therefore, most people lack preexisting immunity to anthrax.

Research on the anthrax toxin tumor therapeutic progresses in several directions [147]. First, the monomeric PA can be retargeted toward the tumor-cell-specific receptors. The approach feasibility was shown in a study when the C-terminus of the PA-WT was fused to the 410–419 residues of the human $p62^{c\text{-}Myc}$ epitope using a $(G_2S)_2$ linker to redirect PA to p62 (c-Myc)-specific hybridoma cell line 9E10 [148]. As a result, the PA-c-Myc variant interacted with the ac-Myc IgG receptor but was still active against its endogenous receptors. The later binding had to be inhibited by the addition of a competitive inhibitor SNKEΔFF made of 1–254 residues of LF and the ADP-ribosylation domain of Pseudomonas exotoxin. In another study, a double N682A and D683A mutation [149] was introduced into domain 4 of PA (mPA) with a goal to disrupt its receptor-binding activity [150]. The C terminus of resulting mutated PA protein was then fused to one of two heterologous receptor-binding proteins, human epidermal growth factor or the receptor-binding domain of the diphtheria toxin. Importantly, the resulting PA variants with the altered receptor specificity were still able to oligomerize and eventually mediate the active components of the toxin cell entry. A similar approach was also successfully tested to retarget the anthrax toxin to the HER2 tyrosine kinase receptor, which is a marker expressed at the surface of many breast and ovarian tumor cells [151]. In particular $ZHER_{2:342}$ [152] affibody, specific for the HER2 receptor, was fused to the C terminus of receptor recognition-deficient PA. The affibodies are small (~6 kDa), pH and thermo-stable targeting polypeptides derived from the Z domain of *Staphylococcus aureus* protein A, which lack Cys residues, are able to fold independently and reversibly and may be rapidly evolved *in vitro* to monoclonal-antibody-like levels of affinity [153]. The resulting mPA-ZHER2 variant displayed no off-target toxicity against HER2-negative cell lines and was effective in delivering LF constructs to a panel of different HER2-positive tumor cell lines [151,154]. It was also demonstrated that by introducing certain mutations, in particular I656Q, it is possible to redesign PA to make it CMG2 but not TEM8 specific [155]. The endogenous CMG2 receptor was shown to play an important role in tumor targeting by the tailored anthrax toxin components [156,157]. More recently, PA was reengineered by fusing a designed ankyrin repeat protein to ablate binding to its own receptor and secure binding to a receptor of choice [158]. This modification allowed for the prepore/pore transition to be delayed taking place in late endosomes specifically. As a result, the variants could have been administered at much higher concentrations, without showing any toxicity, which is very beneficial for the desired cargo intracellular delivery.

The second approach to tailor PA is to substitute the furin cleavage site with cleavage sites for cancer-cell-specific proteases, which are overexpressed in a variety of tumor tissues and tumor cell lines [159]. In 2000, by constructing two PA variants, in which the furin protease recognition site was replaced by matrix metalloproteases (MMP) susceptible GPLGMLSQ (PA-L1) and GPLGLWAQ (PA-L2) sequences [160], Liu et al. showed that these MMP-targeted PA constructs can be activated selectively at the surface of MMP-overexpressing tumor cells. The

tailored PA -L1 and PA-L2 oligomers were successfully used to deliver LF variants to different tumor cells, including human fibrosarcoma, breast cancer, melanoma, and thyroid carcinoma [160–165]. In another study, the furin protease activation site in PA was replaced by urokinase plasminogen activator (uPA, not to be confused with PA) recognition GSGRSA and GSGKSA sequences to get PA-U2 and PA-U3 constructs [166]. Eventually, PA specificity was increased by the design of its mutated PA-L1 and PA-U2 variants, which required both MMP and uPA proteases to form functional heteroheptamers [167]. The approach was further refined by constructing the PA-D512K mutants that exclusively and selectively formed heterooctamers (Fig. 3) with either PA-GN or PA-NS mutants (describe in Section 3.2) [51]. More recently to low the cost and simplify clinical testing, PA-L1 and PA-U2 constructs were chemically conjugated to create cross-linked dimers, which also could only assemble into the octameric complexes [168].

The third direction relies on the unique ability of PA_{63} channel translocation machinery to transport not only native LF and EF components but a diversity of engineered LF_N- and EF_N-based variants known as fusion proteins constructed using the so-called "cut and paste" approach [147,169,170]. To increase the therapeutic benefit of the natural LF and EF components, the chimeric proteins were designed, which contained the PA_{63} binding N-terminal LF_N and EF_N domains fused with the so-called toxophores, namely Pseudomonas exotoxin A enzymatic domain, Shiga toxin enzymatic domain, diphtheria toxin A chain, tetanus toxin light chain, *Clostridium difficile* B toxin glycosylating domain, *Haemophilus ducreyi* cytolethal distending toxin B subunit, Bcl-XL protein, ricin toxin A chain, flagellin, beta-lactamase, A isoform of the enzyme nucleoside diphosphate kinase, antisense peptide nucleic acids, and epidermal growth factor [151,171–183]. Many of these constructs were successfully delivered into the cytosol when applied together with the WT or mutated PA. Some of those that failed, likely were not capable to unfold in the acidic endosomal environment to translocate through the channel. Detailed description of different approaches designed to overcome this and other challenges is beyond the scope of this review and could be found elsewhere [147].

3.8. Clostridial binary toxin channels as close analogs to PA_{63}

The anthrax toxin is a tripartite exotoxin with two A components, LF targeting MAPKKs and Nlrp1 and EF leading to increase in cAMP level. Both components are actively transported into the cytosol by a sole B component, PA. Remarkably, many properties of PA, and especially of PA_{63} channel, resemble those of the B components of a family of clostridial binary exotoxins [184]. They include C2 toxin of *Clostridium botulinum* and iota toxin of *Clostridioides difficile*. The B components (C2II and Ib) of these toxins were reported to form stable and well-defined ion channels when incorporated into PLMs [185–189]. At the same time, the A components of the toxins (C2I and Ia) act through mono-ADP-ribosylation of G-actin at arginine-177, which triggers the actin cytoskeleton distraction and caspase-dependent cell death [190–194]. Many details of the channel-mediated cellular uptake of the C2 and iota toxins are similar to the anthrax toxin. PA, C2II, and Ib share from 27% to 38% of amino acid homology, mostly localized within the two central domains, domain 2 involved in the transmembrane channel formation and A component transport and domain 3 important for heptamer formation. In contrast to PA_{63}, there were no octameric C2II and Ib variants reported. There is a little homology between PA, C2II, and Ib's domains 1 and 4, which are responsible respectively for the A component and cellular receptor binding. This finding is not entirely unexpected considering that the B components are evolved to bind to the different cellular receptors and dock substantially distinct A components of the binary exotoxins [195–199]. The C2II binds asparagine-linked carbohydrates at the cell surface receptor [195] and Ib the lipolysis-stimulated lipoprotein receptor [197,200]. Similarly to PA, after receptor binding and proteolytic activation, the truncated B components of the C2 and iota toxins (C2IIa and Ib) form ring-shaped heptameric prepores on the host cell surface [201–203]. Following the C2I and Ia components binding, the binary toxin complexes are endocytosed where C2IIa and Ib incorporate into endosomal membranes forming ion channels responsible for C2I and Ia component translocation into the cytosol [185,201,204–208]. Recently reported high-resolution cryo-EM structure of the heptameric Ib channel [209] showed that the overall Ib structure is similar to PA_{63} (Fig. 12A). Briefly, both in PA_{63} and Ib domain 2 forms an elongated 14-stranded β barrel stem with ~15 Å inner diameter. The structure showed Ib having one clamp and four constriction sites. The ϕ-clamp configuration is also preserved in Ib; earlier residues F454 in Ib and F428 in C2IIa were shown to be critical for the binary toxin activity [210,211]. Importantly, even though the overall structure, constriction sites, and the channel lumen electrostatic potential were similar between Ib and PA_{63}, Ia binding mode was unique. In contrast to the reported 3:7 and 4:8 LF/EF:PA_{63} complex stoichiometries [29,30,44,45,212–214], only one Ia component was found to bind to Ib (see ref. [209] for further details of the reported structures and their comparison with the anthrax toxin complexes). Similarly, in the related *Clostridioides difficile* binary transferase toxin (CDT) only a single molecule of an enzymatic CDTa component was shown to interact with a CDTb channel-forming component [215]. We chose not to discuss the CDTb channels in the current review because of ambiguity about their variants [216].

In PLMs, the activated C2IIa and Ib components were shown to form cation-selective channels with ion conductance changing as Ib < C2IIa < PA_{63} (Fig. 12B) [57,185,186,205]. While the C2IIa channel conductance also followed the non-linear dependence on the bathing solution concentration, the Ib channel conductance dependence was close to linear (Fig. 12C). Remarkably, fast current fluctuations described by a $1/f$ noise spectrum discussed earlier for PA_{63}, were also observed in C2IIa and Ib single-channel recordings (Fig. 12B). While all three channels remained selective for cations, the cationic selectivity changed as Ib < C2IIa < PA_{63}; yet with all three channels, the selectivity was systematically smaller when the salt concentrations were higher at the *trans* compartment of the bilayer chamber [106]. Many small-molecule and multivalent cationic blockers, successfully tested against PA_{63} channels in PLMs, also were shown to reversibly block C2IIa and Ib channels; their binding activity changed as PA_{63} > C2IIa ≫ Ib [57,67,121,122,124,186,205,211,217–219]. While in *in vitro* PLM measurements, C2IIa and Ib channel block by their C2I and Ia components was reported [186,206], the enzymatic factor translocation experiments were so far unsuccessful. At the same time, Kronhardt et al. reported that in PLM PA_{63} is able to bind C2I, while C2IIa binds both LF and EF [220]. PA was also effective in promoting the non-native enzymatic C2I component uptake into target endothelial cells, where it caused actin modification and cell rounding.

4. Concluding remarks

Our current understanding of the anthrax toxin internalization, while still being incomplete, is arguably unparalleled in the bacterial exotoxin field. Many molecular details of channel-mediated anthrax lethal and edema toxin uptake were clarified largely because of the well-thought-out and neat experiments performed using the PLM technique. The powerful method allows for direct monitoring of changes in the ion current through the anthrax toxin PA_{63} channel in response to its interaction with LF and EF [32], the enzymatic toxin release, interpreted as the translocation [33], and channel inhibition by the blockers [56,67,115]. New knowledge on the anthrax toxin uptake is essential not only for the development of the toxin inhibitors but also for the design of the effective targeted toxin constructs for cancer therapies [147]. Nevertheless, there are several peculiar properties of the anthrax toxin, and the PA_{63} channel explicitly, that, in our view, need clarification. Particularly, while the channel-mediated enzymatic factor translocation was investigated and interpreted under a variety of experimental conditions (Section 3.4) (reviewed in ref. [100]), many

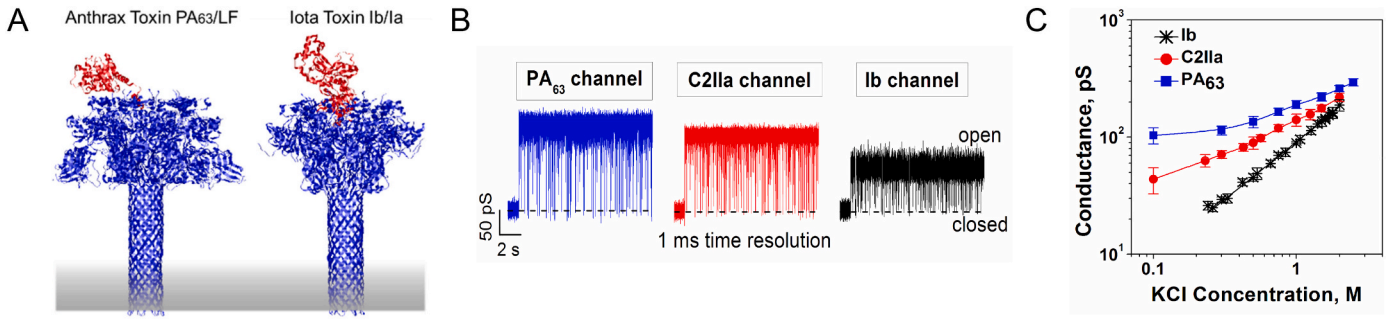

Fig. 12. Binary bacterial anthrax, C2, and iota toxin channel-forming components. ***(A)*** Cryo-EM structures of PA_{63} (PDB ID: 6PSN [46]) and Ib (PDB ID: 6KLW [209]) channels in complex with one molecule of LF and Ia correspondingly. ***(B)*** *Ion* currents through single PA_{63}, C2IIa, and Ib channels show fast fluctuations between their completely open and closed states. ***(C)*** The single-channel conductance *vs.* KCl concentration dependence is close to linear for Ib but shows significant deviations from linearity for the PA_{63} and C2IIa. *(B)* and *(C)* are reprinted with permission from ref. [106].

aspects of the PA_{63} channel behavior are yet to be explained and whether there is a link between these properties and the channel translocase function is undetermined. After the resolved cryo-EM structure of the $(PA_{63})_7$ has shown the channel limiting diameter being as narrow as 6 Å [5], the idea of PA_{63} channel regions dynamically switching between several conformational states quickly gained popularity [59,92,93]. At the same time, despite the notional ability of the cryo-EM technology to capture various short-lived transient protein conformations, only a single high-resolution 'frozen flower on a stem' structure of the anthrax toxin channel has so far been reported. However, the actual model membrane PA_{63} channel dynamic is very complex showing three distinct modes of behavior: *(1)* two open (max and *main*) conductance states (Section 3.3.1) (Fig. 4), *(2)* voltage-gating (Section 3.3.2) (Fig. 5), and *(3)* $1/f$ noise (Section 3.3.3) (Figs. 6) [39,59,115]. Notably, voltage gating and $1/f$ fluctuations are observed in the channel-forming components of clostridial binary C2 and iota toxins, which share functional and structural similarities with the anthrax toxin channel (Section 3.8) (Fig. 12). Similar to PA_{63}, they are evolved to translocate the enzymatic components of the toxins into the cytosol. While the highly asymmetric voltage gating is easy to rule out, we cannot help but wonder whether the $1/f$ noise property, absent in the PA_{63}-F427A mutant, is linked to the translocase activity of the binary toxin channels. The unique properties of PA_{63} also include the two patterns of the channel conductance change with KCl concentration observed at pH 6.5 and 4.5 [11] (Section 3.3.4) (Fig. 7A), the atypically strong effect of the PEG addition on the channel conductance (Sections 3.3.1 and 3.3.5) (Figs. 4F and 8) [64], and the dependence of the channel-forming activity, structural dynamics, small ion transport characteristics, and enzymatic factor binding on the membrane lipid composition (Section 3.6) (Fig. 11) [69]. It remains to be seen if these recent *in vitro* findings are associated in any way with the anthrax toxin *in vivo* assembly and translocation.

Abbreviations

PA	protective antigen
PA_{83}	83-kDa full-length PA
PA_{20}	20-kDa fragment cleaved off protective antigen
PA_{63}	63-kDa fragment of protective antigen
$(PA_{63})_7$	PA_{63} heptamer
$(PA_{63})_8$	PA_{63} octamer
αHL	α-hemolysin
OmpF	outer membrane protein F
VDAC	voltage dependent anion channel
PLM	planar lipid membranes
LF	lethal factor
EF	edema factor
LT	lethal toxin
ET	edema toxin
MAPKKs	mitogen-activated protein kinase kinases
cAMP	cyclic adenosine monophosphate
TEM8/ANTXR1	tumor endothelial marker-8 receptor
CMG2/ANTXR2	capillary morphogenesis gene-2 receptor
EE	early endosome
LE	late endosome
WT	wild type
PEG400	poly(ethylene glycol), with a molecular weight of 400 Da
βCD	β-cyclodextrin
AmPrβCD	per-6-(3-aminopropylthio)-β-cyclodextrin
AMBnTαCD	per-6-S-(3-aminomethyl) benzyl-α-cyclodextrin
AMBnTβCD	per-6-S-(3-aminomethyl) benzyl-β-cyclodextrin
AMBnTγCD	per-6-S-(3-aminomethyl) benzyl-γ-cyclodextrin
MTP	methyltriphenylphosphonium ion
G0-PAMAM	G0 poly(amidoamine) dendrimer
MTPP	methyltriphenylphosphonium chloride
DPhPS	1,2-diphytanoyl-sn-glycero-3-phospho-L-serine
DPhPC	1,2-diphytanoyl-sn-glycero-3-phosphocholine
DOPC	1,2-dioleoyl-sn-glycero-3-phosphocholine
DOPS	1,2-dioleoyl-sn-glycero-3-phospho-L-serine
DOPE	1,2-dioleoyl-sn-glycero-3-phosphoethanolamine
DOBMP	bis(monooleoylglycero)phosphate (S, R isomer)
E_{rev}	reversal potential
Phe	phenylalanine
Ib	the binding/translocation components of *Clostridioides botulinum* iota-toxin
Ia	the enzymatic components of *Clostridioides botulinum* iota-toxin
C2II	the binding/translocation components of *Clostridium botulinum* C2 toxin
C2I	the enzymatic components of *Clostridium botulinum* C2 toxin
MMP	matrix metalloproteases
RMSF	root-mean-square fluctuation
Cryo-EM	cryo-electron microscopy
MD	molecular dynamics
SASA	solvent accessible surface area

Declaration of competing interest

The authors declare the following financial interests/personal relationships which may be considered as potential competing interests: Ekaterina Nestorovich reports financial support was provided by National Institutes of Health.

Acknowledgments

The project was financially supported by NIAID of the NIH under

award number 1R15AI099897-01A1 (to EMN).

References

[1] L. Song, M.R. Hobaugh, C. Shustak, S. Cheley, H. Bayley, J.E. Gouaux, Structure of staphylococcal alpha-hemolysin, a heptameric transmembrane pore, Science 274 (5294) (1996) 1859–1866.

[2] J.J. Kasianowicz, E. Brandin, D. Branton, D.W. Deamer, Characterization of individual polynucleotide molecules using a membrane channel, Proc. Natl. Acad. Sci. U. S. A. 93 (24) (1996) 13770–13773.

[3] J.J. Kasianowicz, A.K. Balijepalli, J. Ettedgui, J.H. Forstater, H. Wang, H. Zhang, J.W. Robertson, Analytical applications for pore-forming proteins, Biochim. Biophys. Acta 1858 (3) (2015) 593–606.

[4] H. Bayley, Nanopore sequencing: from imagination to reality, Clin. Chem. 61 (1) (2015) 25–31.

[5] J. Jiang, B.L. Pentelute, R.J. Collier, Z.H. Zhou, Atomic structure of anthrax protective antigen pore elucidates toxin translocation, Nature 521 (7553) (2015) 545–549.

[6] N.S. Duesbery, C.P. Webb, S.H. Leppla, V.M. Gordon, K.R. Klimpel, T. D. Copeland, N.G. Ahn, M.K. Oskarsson, K. Fukasawa, K.D. Paull, G.F., Vande woude, proteolytic inactivation of MAP-kinase-kinase by anthrax lethal factor, Science 280 (5364) (1998) 734–737.

[7] G. Vitale, L. Bernardi, G. Napolitani, M. Mock, C. Montecucco, Susceptibility of mitogen-activated protein kinase kinase family members to proteolysis by anthrax lethal factor, Biochem. J. 352 (Pt 3) (2000) 739–745.

[8] J.L. Levinsohn, Z.L. Newman, K.A. Hellmich, R. Fattah, M.A. Getz, S. Liu, I. Sastalla, S.H. Leppla, M. Moayeri, Anthrax lethal factor cleavage of Nlrp1 is required for activation of the inflammasome, PLoS Pathog. 8 (3) (2012) e1002638.

[9] S.H. Leppla, Anthrax toxin edema factor: a bacterial adenylate cyclase that increases cyclic AMP concentrations of eukaryotic cells, Proc. Natl. Acad. Sci. U. S. A. 79 (10) (1982) 3162–3166.

[10] F. Dumetz, G. Jouvion, H. Khun, I.J. Glomski, J.P. Corre, C. Rougeaux, W.J. Tang, M. Mock, M. Huerre, P.L. Goossens, Noninvasive imaging technologies reveal edema toxin as a key virulence factor in anthrax, Am. J. Pathol. 178 (6) (2011) 2523–2535.

[11] N. Kalu, A. Alcaraz, G. Yamini, S.M. Abolfath, L. Lucas, C. Kenney, V.M. Aguilella, E.M. Nestorovich, Effect of endosomal acidification on small ion transport through the anthrax toxin PA63 channel, FEBS Lett. 591 (2017) 3481–3492.

[12] L. Abrami, S. Liu, P. Cosson, S.H. Leppla, F.G. van der Goot, Anthrax toxin triggers endocytosis of its receptor via a lipid raft-mediated clathrin-dependent process, J. Cell Biol. 160 (3) (2003) 321–328.

[13] A.M. Friedlander, Macrophages are sensitive to anthrax lethal toxin through an acid-dependent process, J. Biol. Chem. 261 (16) (1986) 7123–7126.

[14] K.A. Bradley, J. Mogridge, M. Mourez, R.J. Collier, J.A. Young, Identification of the cellular receptor for anthrax toxin, Nature 414 (6860) (2001) 225–229.

[15] H.M. Scobie, G.J. Rainey, K.A. Bradley, J.A. Young, Human capillary morphogenesis protein 2 functions as an anthrax toxin receptor, Proc. Natl. Acad. Sci. U. S. A. 100 (9) (2003) 5170–5174.

[16] G.J. Rainey, D.J. Wigelsworth, P.L. Ryan, H.M. Scobie, R.J. Collier, J.A. Young, Receptor-specific requirements for anthrax toxin delivery into cells, Proc. Natl. Acad. Sci. U. S. A. 102 (37) (2005) 13278–13283.

[17] J.T. Wolfe, B.A. Krantz, G.J. Rainey, J.A. Young, R.J. Collier, Whole-cell voltage clamp measurements of anthrax toxin pore current, J. Biol. Chem. 280 (47) (2005) 39417–39422.

[18] G. van der Goot, J.A. Young, Receptors of anthrax toxin and cell entry, Mol. Asp. Med. 30 (6) (2009) 406–412.

[19] S. Liu, D. Crown, S. Miller-Randolph, M. Moayeri, H. Wang, H. Hu, T. Morley, S. H. Leppla, Capillary morphogenesis protein-2 is the major receptor mediating lethality of anthrax toxin in vivo, Proc. Natl. Acad. Sci. U. S. A. 106 (30) (2009) 12424–12429.

[20] D.J. Wigelsworth, B.A. Krantz, K.A. Christensen, D.B. Lacy, S.J. Juris, R.J. Collier, Binding stoichiometry and kinetics of the interaction of a human anthrax toxin receptor, CMG2, with protective antigen, J. Biol. Chem. 279 (22) (2004) 23349–23356.

[21] S. Friebe, F.G. van der Goot, J. Bürgi, The ins and outs of anthrax toxin, Toxins (Basel) 8 (3) (2016).

[22] J. Sun, P. Jacquez, Roles of anthrax toxin receptor 2 in anthrax toxin membrane insertion and pore formation, Toxins (Basel) 8 (2) (2016) 34.

[23] O.A. Sergeeva, F.G. van der Goot, Converging physiological roles of the anthrax toxin receptors, F1000Res 8 (2019).

[24] O. Dowling, A. Difeo, M.C. Ramirez, T. Tukel, G. Narla, L. Bonafe, H. Kayserili, M. Yuksel-Apak, A.S. Paller, K. Norton, A.S. Teebi, V. Grum-Tokars, G.S. Martin, G.E. Davis, M.J. Glucksman, J.A. Martignetti, Mutations in capillary morphogenesis gene-2 result in the allelic disorders juvenile hyaline fibromatosis and infantile systemic hyalinosis, Am. J. Hum. Genet. 73 (4) (2003) 957–966.

[25] S. Hanks, S. Adams, J. Douglas, L. Arbour, D.J. Atherton, S. Balci, H. Bode, M. E. Campbell, M. Feingold, G. Keser, W. Kleijer, G. Mancini, J.A. McGrath, F. Muntoni, A. Nanda, M.D. Teare, M. Warman, F.M. Pope, A. Superti-Furga, P. A. Futreal, N. Rahman, Mutations in the gene encoding capillary morphogenesis protein 2 cause juvenile hyaline fibromatosis and infantile systemic hyalinosis, Am. J. Hum. Genet. 73 (4) (2003) 791–800.

[26] V. Stránecký, A. Hoischen, H. Hartmannová, M.S. Zaki, A. Chaudhary, E. Zudaire, L. Nosková, V. Barešová, A. Pristoupilová, K. Hodanová, J. Sovová, H. Hulková, L. Piherová, J.Y. Hehir-Kwa, D. de Silva, M.P. Senanayake, S. Farrag, J. Zeman, P. Martásek, A. Baxová, H.H. Afifi, B. St Croix, H.G. Brunner, S. Temtamy, S. Kmoch, Mutations in ANTXR1 cause GAPO syndrome, Am. J. Hum. Genet. 92 (5) (2013) 792–799.

[27] S.S. Molloy, P.A. Bresnahan, S.H. Leppla, K.R. Klimpel, G. Thomas, Human furin is a calcium-dependent serine endoprotease that recognizes the sequence arg-X-X-arg and efficiently cleaves anthrax toxin protective antigen, J. Biol. Chem. 267 (23) (1992) 16396–16402.

[28] C. Petosa, R.J. Collier, K.R. Klimpel, S.H. Leppla, R.C. Liddington, Crystal structure of the anthrax toxin protective antigen, Nature 385 (6619) (1997) 833–838.

[29] A.F. Kintzer, K.L. Thoren, H.J. Sterling, K.C. Dong, G.K. Feld, I.I. Tang, T. T. Zhang, E.R. Williams, J.M. Berger, B.A. Krantz, The protective antigen component of anthrax toxin forms functional octameric complexes, J. Mol. Biol. 392 (3) (2009) 614–629.

[30] J. Mogridge, K. Cunningham, R.J. Collier, Stoichiometry of anthrax toxin complexes, Biochemistry 41 (3) (2002) 1079–1082.

[31] R.M. Pilpa, M. Bayrhuber, J.M. Marlett, R. Riek, J.A. Young, A receptor-based switch that regulates anthrax toxin pore formation, PLoS Pathog. 7 (12) (2011), e1002354.

[32] S. Zhang, A. Finkelstein, R.J. Collier, Evidence that translocation of anthrax toxin's lethal factor is initiated by entry of its N terminus into the protective antigen channel, Proc. Natl. Acad. Sci. U. S. A. 101 (48) (2004) 16756–16761.

[33] S. Zhang, E. Udho, Z. Wu, R.J. Collier, A. Finkelstein, Protein translocation through anthrax toxin channels formed in planar lipid bilayers, Biophys. J. 87 (6) (2004) 3842–3849.

[34] A.V. Chekanov, A.G. Remacle, V.S. Golubkov, V.S. Akatov, S. Sikora, A. Y. Savinov, M. Fugere, R. Day, D.V. Rozanov, A.Y. Strongin, Both PA63 and PA83 are endocytosed within an anthrax protective antigen mixed heptamer: a putative mechanism to overcome a furin deficiency, Arch. Biochem. Biophys. 446 (1) (2006) 52–59.

[35] I. Chvyrkova, X.C. Zhang, S. Terzyan, Lethal factor of anthrax toxin binds monomeric form of protective antigen, Biochem. Biophys. Res. Commun. 360 (3) (2007) 690–695.

[36] L. Abrami, M. Lindsay, R.G. Parton, S.H. Leppla, F.G. van der Goot, Membrane insertion of anthrax protective antigen and cytoplasmic delivery of lethal factor occur at different stages of the endocytic pathway, J. Cell Biol. 166 (5) (2004) 645–651.

[37] L. Abrami, L. Brandi, M. Moayeri, M.J. Brown, B.A. Krantz, S.H. Leppla, F.G. van der Goot, Hijacking multivesicular bodies enables long-term and exosome-mediated long-distance action of anthrax toxin, Cell Rep. 5 (4) (2013) 986–996.

[38] B.J. Nablo, R.G. Panchal, S. Bavari, T.L. Nguyen, R. Gussio, W. Ribot, A. Friedlander, D. Chabot, J.E. Reiner, J.W. Robertson, A. Balijepalli, K. M. Halverson, J.J. Kasianowicz, Anthrax toxin-induced rupture of artificial lipid bilayer membranes, J. Chem. Phys. 139 (6) (2013), 065101.

[39] R.O. Blaustein, T.M. Koehler, R.J. Collier, A. Finkelstein, Anthrax toxin: channel-forming activity of protective antigen in planar phospholipid bilayers, Proc. Natl. Acad. Sci. U. S. A. 86 (7) (1989) 2209–2213.

[40] R.O. Blaustein, E.J. Lea, A. Finkelstein, Voltage-dependent block of anthrax toxin channels in planar phospholipid bilayer membranes by symmetric tetraalkylammonium ions. Single-channel analysis, J. Gen. Physiol. 96 (5) (1990) 921–942.

[41] R.O. Blaustein, A. Finkelstein, Voltage-dependent block of anthrax toxin channels in planar phospholipid bilayer membranes by symmetric tetraalkylammonium ions. Effects on macroscopic conductance, J. Gen. Physiol. 96 (5) (1990) 905–919.

[42] R.O. Blaustein, A. Finkelstein, Diffusion limitation in the block by symmetric tetraalkylammonium ions of anthrax toxin channels in planar phospholipid bilayer membranes, J. Gen. Physiol. 96 (5) (1990) 943–957.

[43] A. Finkelstein, The channel formed in planar lipid bilayers by the protective antigen component of anthrax toxin, Toxicology 87 (1–3) (1994) 29–41.

[44] C. Antoni, D. Quentin, A.E. Lang, K. Aktories, C. Gatsogiannis, S. Raunser, Cryo-EM structure of the fully-loaded asymmetric anthrax lethal toxin in its heptameric pre-pore state, PLoS Pathog. 16 (8) (2020), e1008530.

[45] K. Zhou, S. Liu, N.J. Hardenbrook, Y. Cui, B.A. Krantz, Z.H. Zhou, Atomic structures of anthrax prechannel bound with full-length lethal and edema factors, Structure 28 (8) (2020) 879–887.e3.

[46] N.J. Hardenbrook, S. Liu, K. Zhou, K. Ghosal, Z. Hong Zhou, B.A. Krantz, Atomic structures of anthrax toxin protective antigen channels bound to partially unfolded lethal and edema factors, Nat. Commun. 11 (1) (2020) 840.

[47] R.C. Liddington, Assembly and function of the anthrax toxin protein translocation complex, Subcell Biochem. 96 (2021) 563–577.

[48] G.K. Feld, K.L. Thoren, A.F. Kintzer, H.J. Sterling, I.I. Tang, S.G. Greenberg, E. R. Williams, B.A. Krantz, Structural basis for the unfolding of anthrax lethal factor by protective antigen oligomers, Nat. Struct. Mol. Biol. 17 (11) (2010) 1383–1390.

[49] G.K. Feld, A.F. Kintzer, K.L. Tang II, B.A.Krantz Thoren, Domain flexibility modulates the heterogeneous assembly mechanism of anthrax toxin protective antigen, J. Mol. Biol. 415 (1) (2012) 159–174.

[50] H.J. Sterling, A.F. Kintzer, G.K. Feld, C.A. Cassou, B.A. Krantz, E.R. Williams, Supercharging protein complexes from aqueous solution disrupts their native conformations, J. Am. Soc. Mass Spectrom. 23 (2) (2012) 191–200.

[51] D.D. Phillips, R.J. Fattah, D. Crown, Y. Zhang, S. Liu, M. Moayeri, E.R. Fischer, B. T. Hansen, R. Ghirlando, E.M. Nestorovich, A.N. Wein, L. Simons, S.H. Leppla, C. E. Leysath, Engineering anthrax toxin variants that exclusively form octamers and their application to targeting tumors, J. Biol. Chem. 288 (13) (2013) 9058–9065.

[52] O. Teijido, S.M. Rappaport, A. Chamberlin, S.Y. Noskov, V.M. Aguilella, T. K. Rostovtseva, S.M. Bezrukov, Acidification asymmetrically affects voltage-dependent anion channel implicating the involvement of salt bridges, J. Biol. Chem. 289 (34) (2014) 23670–23682.
[53] A. Alcaraz, E.M. Nestorovich, M. Aguilella-Arzo, V.M. Aguilella, S.M. Bezrukov, Salting out the ionic selectivity of a wide channel: the asymmetry of OmpF, Biophys. J. 87 (2) (2004) 943–957.
[54] O.V. Krasil'nikov, V.I. Ternovskii, B.A. Tashmukhamedov, Properties of conductivity channels induced in phospholipid bilayer membranes by alpha-staphylotoxin, Biofizika 26 (2) (1981) 271–276.
[55] K.I. Lee, S. Jo, H. Rui, B. Egwolf, B. Roux, R.W. Pastor, W. Im, Web interface for brownian dynamics simulation of ion transport and its applications to beta-barrel pores, J. Comput. Chem. 33 (3) (2012) 331–339.
[56] B.A. Krantz, R.A. Melnyk, S. Zhang, S.J. Juris, D.B. Lacy, Z. Wu, A. Finkelstein, R. J. Collier, A phenylalanine clamp catalyzes protein translocation through the anthrax toxin pore, Science 309 (5735) (2005) 777–781.
[57] S.M. Bezrukov, X. Liu, V.A. Karginov, A.N. Wein, S.H. Leppla, M.R. Popoff, H. Barth, E.M. Nestorovich, Interactions of high-affinity cationic blockers with the translocation pores of B. anthracis, C. botulinum, and C. perfringens binary toxins, Biophys. J. 103 (6) (2012) 1208–1217.
[58] E.M. Nestorovich, V.A. Karginov, A.M. Berezhkovskii, S.M. Bezrukov, Blockage of anthrax PA63 pore by a multicharged high-affinity toxin inhibitor, Biophys. J. 99 (1) (2010) 134–143.
[59] D. Das, B.A. Krantz, Peptide- and proton-driven allosteric clamps catalyze anthrax toxin translocation across membranes, Proc. Natl. Acad. Sci. U. S. A. 113 (34) (2016) 9611–9616.
[60] G.K. Feld, M.J. Brown, B.A. Krantz, Ratcheting up protein translocation with anthrax toxin, Protein Sci. 21 (5) (2012) 606–624.
[61] J. Monod, J. Wyman, J.P. Changeux, On the nature of allosteric transitions: a plausible model, J. Mol. Biol. 12 (1965) 88–118.
[62] G. Yamini, E.M. Nestorovich, Relevance of the alternate conductance states of anthrax toxin channel, Proc. Natl. Acad. Sci. U. S. A. 114 (13) (2017) E2545–E2546.
[63] B.A. Krantz, Reply to Yamini and Nestorovich: alternate clamped states of the anthrax toxin protective antigen channel, Proc. Natl. Acad. Sci. U. S. A. (2017) E2547.
[64] B.J. Nablo, K.M. Halverson, J.W. Robertson, T.L. Nguyen, R.G. Panchal, R. Gussio, S. Bavari, O.V. Krasilnikov, J.J. Kasianowicz, Sizing the bacillus anthracis PA63 channel with nonelectrolyte poly(ethylene glycols), Biophys. J. 95 (3) (2008) 1157–1164.
[65] S. Momben Abolfath, M. Kolberg, V.A. Karginov, S.H. Leppla, E.M. Nestorovich, Exploring the nature of cationic blocker recognition by the anthrax toxin channel, Biophys. J. 117 (9) (2019) 1751–1763.
[66] G. Bainbridge, I. Gokce, J.H. Lakey, Voltage gating is a fundamental feature of porin and toxin beta-barrel membrane channels, FEBS Lett. 431 (3) (1998) 305–308.
[67] F. Orlik, B. Schiffler, R. Benz, Anthrax toxin protective antigen: inhibition of channel function by chloroquine and related compounds and study of binding kinetics using the current noise analysis, Biophys. J. 88 (3) (2005) 1715–1724.
[68] D.S. Anderson, R.O. Blaustein, Preventing voltage-dependent gating of anthrax toxin channels using engineered disulfides, J. Gen. Physiol. 132 (3) (2008) 351–360.
[69] N. Kalu, Y. Atsmon-Raz, S.Momben Abolfath, L. Lucas, C. Kenney, S.H. Leppla, D. P. Tieleman, E.M. Nestorovich, in: Effect of Late Endosomal DOBMP Lipid and Traditional Model Lipids of Electrophysiology on the Anthrax Toxin Channel Activity, 2018, pp. 2192–2203.
[70] R. Fuchs, S. Schmid, I. Mellman, A possible role for Na , K -ATPase in regulating ATP-dependent endosome acidification, Proc. Natl. Acad. Sci. U. S. A. 86 (2) (1989) 539–543.
[71] R.W. Van Dyke, J.D. Belcher, Acidification of three types of liver endocytic vesicles: similarities and differences, Am. J. Phys. 266 (1 Pt 1) (1994) 81.
[72] J. Piersol, Random data analysis and measurement procedures, Meas. Sci. Technol. 11 (12) (2000) 1825–1826.
[73] G. Yamini, S. Kanchi, N. Kalu, S. Momben Abolfath, S.H. Leppla, K.G. Ayappa, P. K. Maiti, E.M. Nestorovich, Hydrophobic gating and 1/f noise of the anthrax toxin channel, J. Phys. Chem. B 125 (21) (2021) 5466–5478.
[74] P. Aryal, M.S. Sansom, S.J. Tucker, Hydrophobic gating in ion channels, J. Mol. Biol. 427 (1) (2015) 121–130.
[75] G. Yamini, N. Kalu, S. Momben Abolfath, E.M. Nestorovich, 1/f noise in the anthrax toxin channel, Biophys. J. 114 (3) (2018) 262a.
[76] L. Bocquet, E. Charlaix, Nanofluidics, from bulk to interfaces, Chem. Soc. Rev. 39 (3) (2010) 1073–1095.
[77] R.B. Schoch, J. Han, P. Renaud, Transport phenomena in nanofluidics, Rev. Mod. Phys. 80 (3) (2008) 839–883.
[78] O.V. Krasilnikov, R.Z. Sabirov, V.I. Ternovsky, P.G. Merzliak, J. N. Muratkhodjaev, A simple method for the determination of the pore radius of ion channels in planar lipid bilayer membranes, FEMS Microbiol. Immunol. 5 (1–3) (1992) 93–100.
[79] M.A. Aksoyoglu, R. Podgornik, S.M. Bezrukov, P.A. Gurnev, M. Muthukumar, V. A. Parsegian, Size-dependent forced PEG partitioning into channels: VDAC OmpC, and a-hemolysin, Proc. Natl. Acad. Sci. U. S. A. 113 (32) (2016) 9003–9008.
[80] J. Wesche, J.L. Elliott, P.O. Falnes, S. Olsnes, R.J. Collier, Characterization of membrane translocation by anthrax protective antigen, Biochemistry 37 (45) (1998) 15737–15746.
[81] B.A. Krantz, A. Finkelstein, R.J. Collier, Protein translocation through the anthrax toxin transmembrane pore is driven by a proton gradient, J. Mol. Biol. 355 (5) (2006) 968–979.
[82] K.L. Thoren, E.J. Worden, J.M. Yassif, B.A. Krantz, Lethal factor unfolding is the most force-dependent step of anthrax toxin translocation, Proc. Natl. Acad. Sci. U. S. A. 106 (51) (2009) 21555–21560.
[83] K.L. Thoren, B.A. Krantz, The unfolding story of anthrax toxin translocation, Mol. Microbiol. 80 (3) (2011) 588–595.
[84] S.L. Wynia-Smith, M.J. Brown, G. Chirichella, G. Kemalyan, B.A. Krantz, Electrostatic ratchet in the protective antigen channel promotes anthrax toxin translocation, J. Biol. Chem. 287 (52) (2012) 43753–43764.
[85] A. Schiffmiller, D. Anderson, A. Finkelstein, Ion selectivity of the anthrax toxin channel and its effect on protein translocation, J. Gen. Physiol. 146 (2) (2015) 183–192.
[86] D. Basilio, S.J. Juris, R.J. Collier, A. Finkelstein, Evidence for a proton-protein symport mechanism in the anthrax toxin channel, J. Gen. Physiol. 133 (3) (2009) 307–314.
[87] A. Finkelstein, Proton-coupled protein transport through the anthrax toxin channel, Philos. Trans. R. Soc. Lond. Ser. B Biol. Sci. 364 (1514) (2009) 209–215.
[88] B.E. Janowiak, A. Finkelstein, R.J. Collier, An approach to characterizing single-subunit mutations in multimeric prepores and pores of anthrax protective antigen, Protein Sci. 18 (2) (2009) 348–358.
[89] D. Basilio, P.K. Kienker, S.W. Briggs, A. Finkelstein, A kinetic analysis of protein transport through the anthrax toxin channel, J. Gen. Physiol. 137 (6) (2011) 521–531.
[90] D. Basilio, L.D. Jennings-Antipov, K.S. Jakes, A. Finkelstein, Trapping a translocating protein within the anthrax toxin channel: implications for the secondary structure of permeating proteins, J. Gen. Physiol. 137 (4) (2011) 343–356.
[91] A. Schiffmiller, A. Finkelstein, Ion conductance of the stem of the anthrax toxin channel during lethal factor translocation, J. Mol. Biol. 427 (6 Pt A) (2015) 1211–1223.
[92] K. Ghosal, J.M. Colby, D. Das, S.T. Joy, P.S. Arora, B.A. Krantz, Dynamic phenylalanine clamp interactions define single-channel polypeptide translocation through the anthrax toxin protective antigen channel, J. Mol. Biol. 429 (6) (2017) 900–910.
[93] S. Gonti, W.M. Westler, M. Miyagi, J.G. Bann, Site-specific labeling and (19)F NMR provide direct evidence for dynamic behavior of the anthrax toxin pore ?-clamp structure, Biochemistry 60 (9) (2021) 643–647.
[94] P.K. Gupta, M. Moayeri, D. Crown, R.J. Fattah, S.H. Leppla, Role of N-terminal amino acids in the potency of anthrax lethal factor, PLoS One 3 (9) (2008), e3130.
[95] B.A. Krantz, A.D. Trivedi, K. Cunningham, K.A. Christensen, R.J. Collier, Acid-induced unfolding of the amino-terminal domains of the lethal and edema factors of anthrax toxin, J. Mol. Biol. 344 (3) (2004) 739–756.
[96] B.L. Pentelute, A.P. Barker, B.E. Janowiak, S.B. Kent, R.J. Collier, A semisynthesis platform for investigating structure-function relationships in the N-terminal domain of the anthrax lethal factor, ACS Chem. Biol. 5 (4) (2010) 359–364.
[97] B.L. Pentelute, O. Sharma, R.J. Collier, Chemical dissection of protein translocation through the anthrax toxin pore, Angew. Chem. Int. Ed. Engl. 50 (10) (2011) 2294–2296.
[98] M.J. Brown, K.L. Thoren, B.A. Krantz, Charge requirements for proton gradient-driven translocation of anthrax toxin, J. Biol. Chem. 286 (26) (2011) 23189–23199.
[99] R.J. Collier, Membrane translocation by anthrax toxin, Mol. Asp. Med. 30 (6) (2009) 413–422.
[100] B.A. Krantz, Anthrax toxin protective antigen forms an unusual channel that unfolds and translocates proteins across membranes, in: A.H. Delcour (Ed.), Electrophysiology of Unconventional Channels and Pores, Springer International Publishing, Cham, 2015, pp. 209–240.
[101] R.A. Melnyk, R.J. Collier, A loop network within the anthrax toxin pore positions the phenylalanine clamp in an active conformation, Proc. Natl. Acad. Sci. U. S. A. 103 (26) (2006) 9802–9807.
[102] D. Das, B.A. Krantz, Secondary structure preferences of the anthrax toxin protective antigen translocase, J. Mol. Biol. 429 (5) (2017) 753–762.
[103] J.A. Wagoner, K.A. Dill, Molecular motors: power strokes outperform Brownian ratchets, J. Phys. Chem. B 120 (26) (2016) 6327–6336.
[104] W. Hwang, M. Karplus, Structural basis for power stroke vs Brownian ratchet mechanisms of motor proteins, Proc. Natl. Acad. Sci. U. S. A. 116 (40) (2019) 19777–19785.
[105] A.J. Machen, M.T. Fisher, B.D. Freudenthal, Caught in the Act: Anthrax Toxin Translocation Complex Reveals Insight Into the Lethal Factor Unfolding and Refolding Mechanism, bioRxiv, 2020, 2020.04.20.049601.
[106] E.M. Nestorovich, S.M. Bezrukov, Obstructing toxin pathways by targeted pore blockage, Chem. Rev. 112 (12) (2012) 6388–6430.
[107] E.M. Nestorovich, S.M. Bezrukov, Designing inhibitors of anthrax toxin, Expert Opin. Drug Discov. 9 (3) (2014) 299–318.
[108] S. Bezrukov, E. Nestorovich, Inhibitors of Pore-forming Toxins, Forth edition, 2015.
[109] G. Yamini, E.M. Nestorovich, Multivalent inhibitors of channel-forming bacterial toxins, Curr. Top. Microbiol. Immunol. 406 (2016) 199–227.
[110] B.R. Sellman, M. Mourez, R.J. Collier, Dominant-negative mutants of a toxin subunit: an approach to therapy of anthrax, Science 292 (5517) (2001) 695–697.
[111] Y. Singh, H. Khanna, A.P. Chopra, V. Mehra, A dominant negative mutant of bacillus anthracis protective antigen inhibits anthrax toxin action in vivo, J. Biol. Chem. 276 (25) (2001) 22090–22094.

[112] M. Yan, R.J. Collier, Characterization of dominant-negative forms of anthrax protective antigen, Mol. Med. 9 (1–2) (2003) 46–51.
[113] S. Cao, A. Guo, Z. Liu, Y. Tan, G. Wu, C. Zhang, Y. Zhao, H. Chen, Investigation of new dominant-negative inhibitors of anthrax protective antigen mutants for use in therapy and vaccination, Infect. Immun. 77 (10) (2009) 4679–4687.
[114] B.E. Janowiak, A. Fischer, R.J. Collier, Effects of introducing a single charged residue into the phenylalanine clamp of multimeric anthrax protective antigen, J. Biol. Chem. 285 (11) (2010) 8130–8137.
[115] V.A. Karginov, E.M. Nestorovich, M. Moayeri, S.H. Leppla, S.M. Bezrukov, Blocking anthrax lethal toxin at the protective antigen channel by using structure-inspired drug design, Proc. Natl. Acad. Sci. U. S. A. 102 (42) (2005) 15075–15080.
[116] V.A. Karginov, E.M. Nestorovich, F. Schmidtmann, T.M. Robinson, A. Yohannes, N.E. Fahmi, S.M. Bezrukov, S.M. Hecht, Inhibition of S. aureus alpha-hemolysin and B. anthracis lethal toxin by beta-cyclodextrin derivatives, Bioorg. Med. Chem. 15 (16) (2007) 5424–5431.
[117] M.V. Backer, V. Patel, B.T. Jehning, K.P. Claffey, V.A. Karginov, J.M. Backer, Inhibition of anthrax protective antigen outside and inside the cell, Antimicrob. Agents Chemother. 51 (1) (2007) 245–251.
[118] M. Moayeri, T.M. Robinson, S.H. Leppla, V.A. Karginov, In vivo efficacy of beta-cyclodextrin derivatives against anthrax lethal toxin, Antimicrob. Agents Chemother. 52 (6) (2008) 2239–2241.
[119] K. Yannakopoulou, L. Jicsinszky, C. Aggelidou, N. Mourtzis, T.M. Robinson, A. Yohannes, E.M. Nestorovich, S.M. Bezrukov, V.A. Karginov, Symmetry requirements for effective blocking of pore-forming toxins: comparative study with alpha-, beta-, and gamma-cyclodextrin derivatives, Antimicrob. Agents Chemother. 55 (7) (2011) 3594–3597.
[120] E.M. Nestorovich, V.A. Karginov, A.M. Berezhkovskii, V.A. Parsegian, S. M. Bezrukov, Kinetics and thermodynamics of binding reactions as exemplified by anthrax toxin channel blockage with a cationic cyclodextrin derivative, Proc. Natl. Acad. Sci. U. S. A. 109 (45) (2012) 18453–18458.
[121] C. Beitzinger, A. Bronnhuber, K. Duscha, Z. Riedl, M. Huber-Lang, R. Benz, G. Hajós, H. Barth, Designed azolopyridinium salts block protective antigen pores in vitro and protect cells from anthrax toxin, PLoS One 8 (6) (2013), e66099.
[122] P. Förstner, F. Bayer, N. Kalu, S. Felsen, C. Förtsch, A. Aloufi, D.Y. Ng, T. Weil, E. M. Nestorovich, H. Barth, Cationic PAMAM dendrimers as pore-blocking binary toxin inhibitors, Biomacromolecules 15 (7) (2014) 2461–2474.
[123] G. Yamini, N. Kalu, E.M. Nestorovich, Impact of dendrimer terminal group chemistry on blockage of the anthrax toxin channel: a single molecule study, Toxins (Basel) 8 (11) (2016).
[124] A.M. Kreidler, R. Benz, H. Barth, Chloroquine derivatives block the translocation pores and inhibit cellular entry of clostridium botulinum C2 toxin and bacillus anthracis lethal toxin, Arch. Toxicol. 91 (3) (2017) 1431–1445.
[125] R. Benz, H. Barth, Toxin transport by A-B type of toxins in eukaryotic target cells and its inhibition by positively charged heterocyclic molecules, Curr. Top. Microbiol. Immunol. 406 (2017) 229–256.
[126] V.A. Karginov, A. Yohannes, T.M. Robinson, N.E. Fahmi, K. Alibek, S.M. Hecht, Beta-cyclodextrin derivatives that inhibit anthrax lethal toxin, Bioorg. Med. Chem. 14 (1) (2006) 33–40.
[127] V.A. Karginov, Cyclodextrin derivatives as anti-infectives, Curr. Opin. Pharmacol. 13 (5) (2013) 717–725.
[128] C. Fasting, C.A. Schalley, M. Weber, O. Seitz, S. Hecht, B. Koksch, J. Dernedde, C. Graf, E.W. Knapp, R. Haag, Multivalency as a chemical organization and action principle, Angew. Chem. Int. Ed. Engl. 51 (42) (2012) 10472–10498.
[129] D.A. Tomalia, J.M.J. Frechet, Discovery of dendrimers and dendritic polymers: a brief historical perspective, J. Polym. Sci. A Polym. Chem. 40 (2002) 2719–2728.
[130] S. Svenson, D.A. Tomalia, Dendrimers in biomedical applications-reflections on the field, Adv. Drug Deliv. Rev. 57 (2005) 2106–2129.
[131] A.M. Woodhull, Ionic blockage of sodium channels in nerve, J. Gen. Physiol. 61 (6) (1973) 687–708.
[132] J. Sunner, K. Nishizawa, P. Kebarle, Ion-solvent molecule interactions in the gas phase. The potassium ion and benzene, J. Phys. Chem. 85 (13) (1981) 1814–1820.
[133] M.A. Petti, T.J. Shepodd, D.A. Dougherty, Design and synthesis of a new class of hydrophobic binding sites, Tetrahedron Lett. 27 (7) (1986) 807–810.
[134] D.A. Dougherty, The cation-p interaction, Acc. Chem. Res. 46 (4) (2013) 885–893.
[135] D.B. Tikhonov, L.G. Magazanik, Voltage dependence of open channel blockade: onset and offset rates, J. Membr. Biol. 161 (1) (1998) 1–8.
[136] W.R. Redwood, F.R. Pfeiffer, J.A. Weisbach, T.E. Thompson, Physical properties of bilayer membranes formed from a synthetic saturated phospholipid in n-decane, Biochim. Biophys. Acta 233 (1) (1971) 1–6.
[137] S. Tristram-Nagle, D.J. Kim, N. Akhunzada, N. Kucerka, J.C. Mathai, J. Katsaras, M. Zeidel, J.F. Nagle, Structure and water permeability of fully hydrated diphytanoylPC, Chem. Phys. Lipids 163 (6) (2010) 630–637.
[138] S. Wang, R.G. Larson, Water channel formation and ion transport in linear and branched lipid bilayers, Phys. Chem. Chem. Phys. 16 (16) (2014) 7251–7262.
[139] M. De Rosa, A. Gambacorta, A. Gliozzi, Structure, biosynthesis, and physicochemical properties of archaebacterial lipids, Microbiol. Rev. 50 (1) (1986) 70–80.
[140] J.C. Mathai, G.D. Sprott, M.L. Zeidel, Molecular mechanisms of water and solute transport across archaebacterial lipid membranes, J. Biol. Chem. 276 (29) (2001) 27266–27271.
[141] V. Cabiaux, C. Wolff, J.M. Ruysschaert, Interaction with a lipid membrane: a key step in bacterial toxins virulence, Int. J. Biol. Macromol. 21 (4) (1997) 285–298.
[142] X.M. Wang, M. Mock, J.M. Ruysschaert, V. Cabiaux, Secondary structure of anthrax lethal toxin proteins and their interaction with large unilamellar vesicles: a fourier-transform infrared spectroscopy approach, Biochemistry 35 (47) (1996) 14939–14946.
[143] S.K. Kochi, I. Martin, G. Schiavo, M. Mock, V. Cabiaux, The effects of pH on the interaction of anthrax toxin lethal and edema factors with phospholipid vesicles, Biochemistry 33 (9) (1994) 2604–2609.
[144] X.M. Wang, R. Wattiez, M. Mock, P. Falmagne, J.M. Ruysschaert, V. Cabiaux, Structure and interaction of PA63 and EF (edema toxin) of bacillus anthracis with lipid membrane, Biochemistry 36 (48) (1997) 14906–14913.
[145] N.I. Zahaf, G. Schmidt, Bacterial toxins for cancer therapy, Toxins (Basel) 9 (8) (2017).
[146] R.G. Panchal, Novel therapeutic strategies to selectively kill cancer cells, Biochem. Pharmacol. 55 (3) (1998) 247–252.
[147] C. Bachran, S.H. Leppla, Tumor targeting and drug delivery by anthrax toxin, Toxins (Basel) 8 (7) (2016).
[148] M. Varughese, A. Chi, A.V. Teixeira, P.J. Nicholls, J.M. Keith, S.H. Leppla, Internalization of a Bacillus anthracis protective antigen-c-Myc fusion protein mediated by cell surface anti-c-Myc antibodies, Mol. Med. 4 (2) (1998) 87–95.
[149] M.J. Rosovitz, P. Schuck, M. Varughese, A.P. Chopra, V. Mehra, Y. Singh, L. M. McGinnis, S.H. Leppla, Alanine-scanning mutations in domain 4 of anthrax toxin protective antigen reveal residues important for binding to the cellular receptor and to a neutralizing monoclonal antibody, J. Biol. Chem. 278 (33) (2003) 30936–30944.
[150] A. Mechaly, A.J. McCluskey, R.J. Collier, Changing the receptor specificity of anthrax toxin, MBio 3 (3) (2012).
[151] A.J. McCluskey, A.J. Olive, M.N. Starnbach, R.J. Collier, Targeting HER2-positive cancer cells with receptor-redirected anthrax protective antigen, Mol. Oncol. 7 (3) (2013) 440–451.
[152] A. Orlova, M. Magnusson, T.L. Eriksson, M. Nilsson, B. Larsson, I. Höidén-Guthenberg, C. Widström, J. Carlsson, V. Tolmachev, S. Ståhl, F.Y. Nilsson, Tumor imaging using a picomolar affinity HER2 binding affibody molecule, Cancer Res. 66 (8) (2006) 4339–4348.
[153] J. Löfblom, J. Feldwisch, V. Tolmachev, J. Carlsson, S. Ståhl, F.Y. Frejd, Affibody molecules: engineered proteins for therapeutic, diagnostic and biotechnological applications, FEBS Lett. 584 (12) (2010) 2670–2680.
[154] A.J. McCluskey, R.J. Collier, Receptor-directed chimeric toxins created by sortase-mediated protein fusion, Mol. Cancer Ther. 12 (10) (2013) 2273–2281.
[155] K.H. Chen, S. Liu, C.E. Leysath, S. Miller-Randolph, Y. Zhang, R. Fattah, T. H. Bugge, S.H. Leppla, Anthrax toxin protective antigen variants that selectively utilize either the CMG2 or TEM8 receptors for cellular uptake and tumor targeting, J. Biol. Chem. 291 (42) (2016) 22021–22029.
[156] S. Liu, J. Liu, Q. Ma, L. Cao, R.J. Fattah, Z. Yu, T.H. Bugge, T. Finkel, S.H. Leppla, Solid tumor therapy by selectively targeting stromal endothelial cells, Proc. Natl. Acad. Sci. U. S. A. 113 (28) (2016) E4079–E4087.
[157] S. Liu, Y. Zhang, B. Hoover, S.H. Leppla, The receptors that mediate the direct lethality of anthrax toxin, Toxins (Basel) 5 (1) (2012) 1–8.
[158] L. Becker, W.P.R. Verdurmen, A. Plückthun, Reengineering anthrax toxin protective antigen for improved receptor-specific protein delivery, BMC Biol. 18 (1) (2020) 100.
[159] K.Y. Choi, M. Swierczewska, S. Lee, X. Chen, Protease-activated drug development, Theranostics 2 (2) (2012) 156–178.
[160] S. Liu, S. Netzel-Arnett, H. Birkedal-Hansen, S.H. Leppla, Tumor cell-selective cytotoxicity of matrix metalloproteinase-activated anthrax toxin, Cancer Res. 60 (21) (2000) 6061–6067.
[161] S. Liu, R.L. Schubert, T.H. Bugge, S.H. Leppla, Anthrax toxin: structures, functions and tumour targeting, Expert. Opin. Biol. Ther. 3 (5) (2003) 843–853.
[162] H.M. Koo, M. VanBrocklin, M.J. McWilliams, S.H. Leppla, N.S. Duesbery, G.F., Vande woude, apoptosis and melanogenesis in human melanoma cells induced by anthrax lethal factor inactivation of mitogen-activated protein kinase kinase, Proc. Natl. Acad. Sci. U. S. A. 99 (5) (2002) 3052–3057.
[163] R.W. Alfano, S.H. Leppla, S. Liu, T.H. Bugge, N.S. Duesbery, A.E. Frankel, Potent inhibition of tumor angiogenesis by the matrix metalloproteinase-activated anthrax lethal toxin: implications for broad anti-tumor efficacy, Cell Cycle 7 (6) (2008) 745–749.
[164] R.W. Alfano, S.H. Leppla, S. Liu, T.H. Bugge, J.M. Ortiz, T.C. Lairmore, N. S. Duesbery, I.C. Mitchell, F. Nwariaku, A.E. Frankel, Inhibition of tumor angiogenesis by the matrix metalloproteinase-activated anthrax lethal toxin in an orthotopic model of anaplastic thyroid carcinoma, Mol. Cancer Ther. 9 (1) (2010) 190–201.
[165] J.M. Schafer, D.E. Peters, T. Morley, S. Liu, A.A. Molinolo, S.H. Leppla, T. H. Bugge, Efficient targeting of head and neck squamous cell carcinoma by systemic administration of a dual uPA and MMP-activated engineered anthrax toxin, PLoS One 6 (5) (2011), e20532.
[166] S. Liu, T.H. Bugge, S.H. Leppla, Targeting of tumor cells by cell surface urokinase plasminogen activator-dependent anthrax toxin, J. Biol. Chem. 276 (21) (2001) 17976–17984.
[167] S. Liu, V. Redeye, J.G. Kuremsky, M. Kuhnen, A. Molinolo, T.H. Bugge, S. H. Leppla, Intermolecular complementation achieves high-specificity tumor targeting by anthrax toxin, Nat. Biotechnol. 23 (6) (2005) 725–730.
[168] E.S. Fischer, S.Liu W.A.t. Campbell R. Ghirlando, Bismaleimide cross-linked anthrax toxin forms functional octamers with high specificity in tumor targeting, Protein Sci. 28 (6) (2019) 1059–1070.
[169] A.E. Frankel, B.L. Powell, N.S. Duesbery, G.F. Vande Woude, S.H. Leppla, Anthrax fusion protein therapy of cancer, Curr. Protein Pept. Sci. 3 (4) (2002) 399–407.

[170] A.E. Rabideau, B.L. Pentelute, Delivery of non-native cargo into mammalian cells using anthrax lethal toxin, ACS Chem. Biol. 11 (6) (2016) 1490–1501.
[171] N. Arora, K.R. Klimpel, Y. Singh, S.H. Leppla, Fusions of anthrax toxin lethal factor to the ADP-ribosylation domain of pseudomonas exotoxin a are potent cytotoxins which are translocated to the cytosol of mammalian cells, J. Biol. Chem. 267 (22) (1992) 15542–15548.
[172] N. Arora, S.H. Leppla, Fusions of anthrax toxin lethal factor with Shiga toxin and diphtheria toxin enzymatic domains are toxic to mammalian cells, Infect. Immun. 62 (11) (1994) 4955–4961.
[173] J.C. Milne, S.R. Blanke, P.C. Hanna, R.J. Collier, Protective antigen-binding domain of anthrax lethal factor mediates translocation of a heterologous protein fused to its amino- or carboxy-terminus, Mol. Microbiol. 15 (4) (1995) 661–666.
[174] N. Arora, L.C. Williamson, S.H. Leppla, J.L. Halpern, Cytotoxic effects of a chimeric protein consisting of tetanus toxin light chain and anthrax toxin lethal factor in non-neuronal cells, J. Biol. Chem. 269 (42) (1994) 26165–26171.
[175] L.M. Spyres, M. Qa'Dan, A. Meader, J.J. Tomasek, E.W. Howard, J.D. Ballard, Cytosolic delivery and characterization of the TcdB glucosylating domain by using a heterologous protein fusion, Infect. Immun. 69 (1) (2001) 599–601.
[176] C. Bachran, R. Hasikova, C.E. Leysath, I. Sastalla, Y. Zhang, R.J. Fattah, S. Liu, S. H. Leppla, Cytolethal distending toxin B as a cell-killing component of tumor-targeted anthrax toxin fusion proteins, Cell Death Dis. 5 (1) (2014), e1003.
[177] X.H. Liu, R.J. Collier, R.J. Youle, Inhibition of axotomy-induced neuronal apoptosis by extracellular delivery of a Bcl-XL fusion protein, J. Biol. Chem. 276 (49) (2001) 46326–46332.
[178] J. von Moltke, N.J. Trinidad, M. Moayeri, A.F. Kintzer, S.B. Wang, N. van Rooijen, C.R. Brown, B.A. Krantz, S.H. Leppla, K. Gronert, R.E. Vance, Rapid induction of inflammatory lipid mediators by the inflammasome in vivo, Nature 490 (7418) (2012) 107–111.
[179] J.P. Hobson, S. Liu, B. Rønø, S.H. Leppla, T.H. Bugge, Imaging specific cell-surface proteolytic activity in single living cells, Nat. Methods 3 (4) (2006) 259–261.
[180] H. Hu, S.H. Leppla, Anthrax toxin uptake by primary immune cells as determined with a lethal factor-beta-lactamase fusion protein, PLoS One 4 (11) (2009), e7946.
[181] I. Felix, S.K. Lomada, H. Barth, T. Wieland, Bacillus anthracis' PA(63) delivers the tumor metastasis suppressor protein NDPK-A/NME1 into breast cancer cells, Int. J. Mol. Sci. 21 (9) (2020).
[182] Z. Lu, B.R. Paolella, N.L. Truex, A.R. Loftis, X. Liao, A.E. Rabideau, M.S. Brown, J. Busanovich, R. Beroukhim, B.L. Pentelute, Targeting cancer gene dependencies with anthrax-mediated delivery of peptide nucleic acids, ACS Chem. Biol. 15 (6) (2020) 1358–1369.
[183] S. Jack, K. Madhivanan, S. Ramadesikan, S. Subramanian, D.F. Edwards II, B. D. Elzey, D. Dhawan, A. McCluskey, E.M. Kischuk, A.R. Loftis, N. Truex, M. Santos, M. Lu, A. Rabideau, B. Pentelute, J. Collier, H. Kaimakliotis, M. Koch, T.L. Ratliff, D.W. Knapp, R.C. Aguilar, A novel, safe, fast and efficient treatment for Her2-positive and negative bladder cancer utilizing an EGF-anthrax toxin chimera, Int. J. Cancer 146 (2) (2020) 449–460.
[184] H. Barth, K. Aktories, M.R. Popoff, B.G. Stiles, Binary bacterial toxins: biochemistry, biology, and applications of common Clostridium and Bacillus proteins, Microbiol. Mol. Biol. Rev. 68 (3) (2004) 373–402, table of contents.
[185] A. Schmid, R. Benz, I. Just, K. Aktories, Interaction of clostridium botulinum C2 toxin with lipid bilayer membranes. Formation of cation-selective channels and inhibition of channel function by chloroquine, J. Biol. Chem. 269 (24) (1994) 16706–16711.
[186] O. Knapp, R. Benz, M. Gibert, J.C. Marvaud, M.R. Popoff, Interaction of Clostridium perfringens iota-toxin with lipid bilayer membranes. Demonstration of channel formation by the activated binding component Ib and channel block by the enzyme component Ia, J. Biol. Chem. 277 (8) (2002) 6143–6152.
[187] O. Knapp, R. Benz, M.R. Popoff, Pore-forming activity of clostridial binary toxins, Biochim. Biophys. Acta 1858 (3) (2016) 512–525.
[188] B.G. Stiles, D.J. Wigelsworth, M.R. Popoff, H. Barth, Clostridial binary toxins: iota and C2 family portraits, Front. Cell. Infect. Microbiol. 1 (2011) 11.
[189] M.R. Popoff, Clostridial pore-forming toxins: powerful virulence factors, Anaerobe 30 (2014) 220–238.
[190] H. Barth, B.G. Stiles, Binary actin-ADP-ribosylating toxins and their use as molecular trojan horses for drug delivery into eukaryotic cells, Curr. Med. Chem. 15 (5) (2008) 459–469.
[191] I. Ohishi, Y. Odagiri, Histopathological effect of botulinum C2 toxin on mouse intestines, Infect. Immun. 43 (1) (1984) 54–58.
[192] K. Aktories, M. Bärmann, I. Ohishi, S. Tsuyama, K.H. Jakobs, E. Habermann, Botulinum C2 toxin ADP-ribosylates actin, Nature 322 (6077) (1986) 390–392.
[193] J. Vandekerckhove, B. Schering, M. Barmann, K. Aktories, Clostridium perfringens iota toxin ADP-ribosylates skeletal muscle actin in Arg-177, FEBS Lett. 225 (1–2) (1987) 48–52.
[194] K. Aktories, A. Wegner, ADP-ribosylation of actin by clostridial toxins, J. Cell Biol. 109 (4 Pt 1) (1989) 1385–1387.
[195] M. Eckhardt, H. Barth, D. Blöcker, K. Aktories, Binding of Clostridium botulinum C2 toxin to asparagine-linked complex and hybrid carbohydrates, J. Biol. Chem. 275 (4) (2000) 2328–2334.
[196] J.C. Marvaud, T. Smith, M.L. Hale, M.R. Popoff, L.A. Smith, B.G. Stiles, Clostridium perfringens iota-toxin: mapping of receptor binding and Ia docking domains on Ib, Infect. Immun. 69 (4) (2001) 2435–2441.
[197] P. Papatheodorou, J.E. Carette, G.W. Bell, C. Schwan, G. Guttenberg, T. R. Brummelkamp, K. Aktories, Lipolysis-stimulated lipoprotein receptor (LSR) is the host receptor for the binary toxin Clostridium difficile transferase (CDT), Proc. Natl. Acad. Sci. U. S. A. 108 (39) (2011) 16422–16427.
[198] M. Takehara, T. Takagishi, S. Seike, M. Oda, Y. Sakaguchi, J. Hisatsune, S. Ochi, K. Kobayashi, M. Nagahama, Cellular entry of Clostridium perfringens iota-toxin and clostridium botulinum C2 toxin, Toxins 9 (8) (2017), https://doi.org/10.3390/toxins9080247.
[199] P. Papatheodorou, K. Aktories, Receptor-binding and uptake of binary actin-ADP-ribosylating toxins, Curr. Top. Microbiol. Immunol. 406 (2017) 119–133.
[200] G. Schmidt, P. Papatheodorou, K. Aktories, Novel receptors for bacterial protein toxins, Curr. Opin. Microbiol. 23 (2015) 55–61.
[201] H. Barth, D. Blocker, J. Behlke, W. Bergsma-Schutter, A. Brisson, R. Benz, K. Aktories, Cellular uptake of Clostridium botulinum C2 toxin requires oligomerization and acidification, J. Biol. Chem. 275 (25) (2000) 18704–18711.
[202] M. Nagahama, M. Umezaki, R. Tashiro, M. Oda, K. Kobayashi, M. Shibutani, T. Takagishi, K. Ishidoh, M. Fukuda, J. Sakurai, Intracellular trafficking of Clostridium perfringens iota-toxin b, Infect. Immun. 80 (10) (2012) 3410–3416.
[203] M. Nagahama, C. Takahashi, K. Aoyanagi, R. Tashiro, K. Kobayashi, Y. Sakaguchi, K. Ishidoh, J. Sakurai, Intracellular trafficking of clostridium botulinum C2 toxin, Toxicon 82 (2014) 76–82.
[204] B.G. Stiles, M.L. Hale, J.C. Marvaud, M.R. Popoff, Clostridium perfringens iota toxin: characterization of the cell-associated iota b complex, Biochem. J. 367 (Pt 3) (2002) 801–808.
[205] C. Bachmeyer, R. Benz, H. Barth, K. Aktories, M. Gilbert, M.R. Popoff, Interaction of clostridium botulinum C2 toxin with lipid bilayer membranes and vero cells: inhibition of channel function by chloroquine and related compounds in vitro and intoxification in vivo, FASEB J. 15 (9) (2001) 1658–1660.
[206] D. Blöcker, K. Pohlmann, G. Haug, C. Bachmeyer, R. Benz, K. Aktories, H. Barth, Clostridium botulinum C2 toxin: low pH-induced pore formation is required for translocation of the enzyme component C2I into the cytosol of host cells, J. Biol. Chem. 278 (39) (2003) 37360–37367.
[207] D. Blöcker, C. Bachmeyer, R. Benz, K. Aktories, H. Barth, Channel formation by the binding component of clostridium botulinum C2 toxin: glutamate 307 of C2II affects channel properties in vitro and pH-dependent C2I translocation in vivo, Biochemistry 42 (18) (2003) 5368–5377.
[208] M. Gibert, J.C. Marvaud, Y. Pereira, M.L. Hale, B.G. Stiles, P. Boquet, C. Lamaze, M.R. Popoff, Differential requirement for the translocation of clostridial binary toxins: iota toxin requires a membrane potential gradient, FEBS Lett. 581 (7) (2007) 1287–1296.
[209] T. Yamada, T. Yoshida, A. Kawamoto, K. Mitsuoka, K. Iwasaki, H. Tsuge, Cryo-EM structures reveal translocational unfolding in the clostridial binary iota toxin complex, Nat. Struct. Mol. Biol. 27 (2020) 288–296.
[210] O. Knapp, E. Maier, E. Waltenberger, C. Mazuet, R. Benz, M.R. Popoff, Residues involved in the pore-forming activity of the Clostridium perfringens iota toxin, Cell. Microbiol. 17 (2) (2015) 288–302.
[211] T. Neumeyer, B. Schiffler, E. Maier, A.E. Lang, K. Aktories, R. Benz, Clostridium botulinum C2 toxin. identification of the binding site for chloroquine and related compounds and influence of the binding site on properties of the C2II channel, J. Biol. Chem. 283 (7) (2008) 3904–3914.
[212] K. Cunningham, D.B. Lacy, J. Mogridge, R.J. Collier, Mapping the lethal factor and edema factor binding sites on oligomeric anthrax protective antigen, Proc. Natl. Acad. Sci. U. S. A. 99 (10) (2002) 7049–7053.
[213] L. Fabre, E. Santelli, D. Mountassif, A. Donoghue, A. Biswas, R. Blunck, D. Hanein, N. Volkmann, R. Liddington, I. Rouiller, Structure of anthrax lethal toxin prepore complex suggests a pathway for efficient cell entry, J. Gen. Physiol. 148 (4) (2016) 313–324.
[214] A.J. Machen, N. Akkaladevi, C. Trecazzi, P.T. O'Neil, S. Mukherjee, Y. Qi, R. Dillard, W. Im, E.P. Gogol, T.A. White, M.T. Fisher, Asymmetric cryo-EM structure of anthrax toxin protective antigen pore with lethal factor N-terminal domain, Toxins (Basel) 9 (10) (2017).
[215] M.J. Sheedlo, D.M. Anderson, A.K. Thomas, D.B. Lacy, Structural elucidation of the Clostridioides difficile transferase toxin reveals a single-site binding mode for the enzyme, Proc. Natl. Acad. Sci. U. S. A. 117 (11) (2020) 6139–6144.
[216] A. Kronhardt, C. Schwan, E. Maier, M.R. Popoff, R. Benz, Clostridium difficile CDT toxin forms two different types of channels in lipid bilayer membranes, BAOJ Chem 3 (2017) 35.
[217] C. Bachmeyer, F. Orlik, H. Barth, K. Aktories, R. Benz, Mechanism of C2-toxin inhibition by fluphenazine and related compounds: investigation of their binding kinetics to the C2II-channel using the current noise analysis, J. Mol. Biol. 333 (3) (2003) 527–540.
[218] L. Schnell, I. Felix, B. Müller, M. Sadi, F. von Bank, P. Papatheodorou, M. R. Popoff, K. Aktories, E. Waltenberger, R. Benz, C. Weichbrodt, M. Fauler, M. Frick, H. Barth, Revisiting an old antibiotic: bacitracin neutralizes binary bacterial toxins and protects cells from intoxication, FASEB J. 33 (4) (2019) 5755–5771.
[219] E.M. Nestorovich, V.A. Karginov, M.R. Popoff, S.M. Bezrukov, H. Barth, Tailored ss-cyclodextrin blocks the translocation pores of binary exotoxins from C. botulinum and C. perfringens and protects cells from intoxication, PLoS One 6 (8) (2011), e23927.
[220] A. Kronhardt, M. Rolando, C. Beitzinger, C. Stefani, M. Leuber, G. Flatau, M. R. Popoff, R. Benz, E. Lemichez, Cross-reactivity of anthrax and C2 toxin: protective antigen promotes the uptake of botulinum C2I toxin into human endothelial cells, PLoS One 6 (8) (2011), e23133.